TITLE PAGE

Crustal seismic structure beneath Portugal and Southern Galicia (Western Iberia) and the role of Variscan inheritance

Idalina Veludo[(1)], Nuno A. Dias[(2,3,*)], Paulo E. Fonseca[(3)], Luís Matias[(3)],Fernando Carrilho[(1)],

Christian Haberland[(4)], Antonio Villaseñor[(5)]

1. Instituto Português do Mar e da Atmosfera, I.P., Rua C ao Aeroporto, 1749-077 Lisbon, Portugal
2. Instituto Superior de Engenharia de Lisboa – ISEL,Instituto Politécnico de Lisboa, R. Conselheiro Emídio Navarro, 1959-007 Lisbon, Portugal
3. Instituto Dom Luiz, Faculdade de Ciências, Universidade de Lisboa, Campo Grande, Ed. C1, Piso 1, 1749-016, Lisbon, Portugal.
4. GeoForschungsZentrum – GFZ, Potsdam, Germany.
5. Institute of Earth Sciences Jaume Almera, ICTJA-CSIC, Barcelona, Spain.

*Corresponding author: Nuno Afonso Dias. Instituto Superior de Engenharia de Lisboa, R. Conselheiro Emídio Navarro, 1959-007 Lisbon, Portugal**.**Tel.:+351 218 317 135; Fax+.:351 218 317 138; E-mails: ndias@adf.isel.pt; nmdias@fc.ul.pt

Other E-mail addresses: Idalina.veludo@ipma.pt(I. Veludo);lmmatias@fc.ul.pt (L. Matias); pefonseca@fc.ul.pt (P. E. Fonseca);fernando.carrilho@ipma.pt (F. Carrilho); haber@gfz-potsdam.de (C. Haberland); antonio.villasenor@csic.es (A. Villaseñor)

1. Introduction

Mainland Portugal comprises most of the Western portion of the Iberian Peninsula, in a complex geodynamic setting associated with the Africa-Eurasia plate boundary. The crust in this area is the result of a complex assemblage history of continental collision and extension: in the Lower Paleozoic, the collision of an unconstrained number of continental blocks resulted in the Variscan Orogeny, the main event of formation of the Iberian lithosphere (e.g. Arenas et al., 2016; Matte, 2001, 1986; Ribeiro et al., 2007a); the subsequent Mesozoic rifting and breakup of the Pangea had a profound effect on the continental crust of the western border of Iberia (Pereira et al., 2016; Ribeiro et al., 1990).

Since the Miocene, the southern interaction between Africa and Iberia is characterized by a diffuse convergent margin that originates a vast area of deformation along southern Iberia. The oblique convergence between the two plates occurs at a slow rate of 3–6 $mmyr^{-1}$ (Fernandes, 2003; Nocquet, 2012; Serpelloni et al., 2007), resulting in a slow deformation regime whose manifestation is a seismicity rate that increases in number and magnitude from north to south (Custódio et al., 2015; Ferrão et al., 2016). While the concentration of the seismicity in the areas closer to the plate boundary was to be expected, the concentration of seismicity along the western Iberian margin and its clustering in some specific places reveals an anomalous pattern not yet fully understood.

The impact and extension of this complex tectonics in the structure of the Iberian lithosphere is still a matter of discussion, especially in its western part beneath Portugal. The existing knowledge relating the observed surface geology and lithospheric deep structures is sparse and sometimes incoherent, the relation between shallow and deep structures and their lateral extension still widely undetermined.

Some questions still pertinent are the role and influence of the several tectonic units, and their contacts, in the present tectonic regime and the stress field observed today and the relation between the anomalous seismicity and associated crustal deformation rates with the inherited structure from past orogenies.

To address these questions, and taking advantage of an accumulated dataset of the seismicity recorded over the last 15 years (cf. Fig.1), we have conducted a local earthquake tomographic study of the crust beneath Portugal.

2. Geological and tectonic framework

The majority of lithological units outcropping in Western Iberia are of Paleozoic age (480-290 Ma) and compose the Iberian Massif or Iberian Autochthonous Terrane, the major outcrop of the SW European Variscides (Fernández et al., 2016; Matte, 2001, 1986; Ribeiro et al., 2007). In Portugal, the Iberian Massif can be divided in four main tectonic units, from north to south (cf. Fig.2): the Galicia-Trás-os-Montes Zone (GTMZ), which consists of a pile of allochthonous thrust sheets, overlying the autochthonous Central Iberian Zone (CIZ), the para-autochtnonous Ossa-Morena Zone (OMZ) and the allochthonous South Portuguese Zone (SPZ) (Arenas et al., 2016b; Dias and Ribeiro, 1995; Ribeiro et al., 2007; Simancas et al., 2001).

The actual tectono-structural outline of the W edge of Iberian Peninsula (Portugal) is the result of three main orogenic events: Cadomian orogeny (660-540 My) (Linnemann et al., 2008; Ribeiro et al., 2009), Variscan Orogeny (380-280 My) (Arenas et al., 2016a; Simancas et al., 2013) and Alpine orogeny (125- 37My) (Jeanniot et al., 2016; Pereira et al., 2016; Pereira and Alves, 2013). The main and most important orogenic event that delineates all the major faults of the territory and tectonic shape is the Variscan event. Characteristically, the Paleozoic collision episode began during the upper Devonian and ended at the Pennsylvanian period (Upper Carboniferous). Since then almost all the reactivation of fault zones takes into account the previous scenario of the three main Variscan tectonic and deformation phases and the last tardi-Variscan fracturation. The Alpine orogeny is controlled by previous orogenic heritage (Miranda et al., 2009; Nance et al., 2010; Pais et al., 2012; Pereira et al., 2016; Wilson, 1966).

The impact of this complex assemblage in the structure of the lithosphere and the topography of some of its inner discontinuities, namely the Moho, has mostly been

addressed through controlled-source experiments (e.g., Banda, 1988; Díaz et al., 1993a; Mueller et al., 1973; Prodehl et al., 1975; Sousa Moreira et al., 1983, 1978; Victor et al., 1980), conducted in the 1970's and 1980's and mainly concentrated in the southern part of the country. Matias (1996) made a synthesis of all deep seismic sounding (DSS) results available in Portugal Mainland, revising all previous data with a common methodology. P-wave velocity models were derived from travel-time inversion (Zelt and Smith, 1992) and amplitudes were controlled by synthetic seismograms (Zelt and Ellis, 1988). That study evidenced the limited spatial coverage of these data and showed features that raised some questions: i) the discrepancy between the velocity model and its gravity anomaly in Vila do Bispo (SW tip of Portugal); ii) the upper crust (down to 10 km depth) is strongly anisotropic in the SPZ; iii) the deep structure and Moho depth in the SPZ show conflicting results between crossing profiles; iv) the OMZ was interpreted as an upper-crust block on top of lower crust blocks from the SPZ and CIZ. In mainland Portugal, there are no S-wave velocity estimates derived from DSS studies. Téllez and Córdoba (1998) estimated S-wave models for the GTMZ (Spanish side) but the seismic character (reflectivity and amplitude of the Moho reflection) is very different from the ones obtained on the Portuguese side, and its generalization to the whole area is uncertain. DSS analysis in Portugal mainland (Matias, 1996) also suggest that the Moho is nearly everywhere a second order discontinuity due to the absence of pre-critical PMP reflections, a result that is at odds with what was observed in the Spanish GTMZ (Téllez et al., 1993).

The DSS results pointed to a Moho discontinuity topography relatively smooth with a progressive thinning from the interior towards the margins, but with some lateral variations. The greater heterogeneity is located in the OMZ, where there is an indication of a crustal thinning relatively to the CIZ and particularly to the SPZ. The models obtained from the majority of the profiles indicate a three-layer crust, the middle-lower crustal levels showing fairly stable results, the main differences being located at the upper crust; where Vp values range from 6.0-6.3 km/s, whereas in the middle and lower crust the typical values are around 6.4-6.5 km/s and 6.6-7.0 km/s respectively. Only in areas of thick sedimentary basins, like the LTV are observed Vp values smaller than 5.0 km/s.

Additional information on the crustal structure has been provided from teleseismic P-Receiver Functions (PRFs) studies. Julia and Mejia (2004) estimated Moho depths and Vp/Vs ratio values at five locations in the Iberian Massif, the Paleozoic core of Iberian Peninsula, obtaining an average crustal thickness of 30 ± 2 km, with an average Vp/Vs ratio of 1.74 ± 0.05. Beneath the Lower Tagus Valley, Salah et al. (2011) estimated Moho depths between 25.5 and 30 km and Vp/Vs ratio variations between 1.65 and 1.81, with an average of 1.75. More recently, in the framework of project WILAS (Dündar et al., 2016), the values of Moho depth and Vp/Vs average crustal ratio were derived covering the entire country; the image provided points to a relatively smooth Moho overall consistent with the DSS values, although with some misfits, whereas the major variations in Vp/Vs appear associated with the structure of the OMZ or beneath the basins at the continental margin.

Discrepancies between DSS velocity models (Matias, 1996) and PRF results (Dündar et al., 2016; Salah et al., 2011), mainly for the Lower Tagus Valley and the SE region of Portugal, also raise the question of how these two datasets can be compared. PRFs are most sensitive to the S-wave velocities and use lower frequencies than controlled source active seismic surveys.

More recently several studies have been performed at smaller scales, mainly in the area of the Lower Tagus Valley (Borges et al., 2016; Carvalho et al., 2016, 2014, 2008; Ghose et al., 2013), due to this region being a potential seismogenic area for Lisbon. These studies show the presence of an uplifted area to the NW of the Tagus Valley and a thick sedimentary basin to the SE.

3. Data selection

The seismicity in Portugal is interpreted nowadays as the result of the convergence regime between the Eurasia and African plates, its rate, depth distribution and magnitude increasing from north to south, the biggest and deeper events being located in the offshore. Inland, the seismicity rarely exceeds magnitude 4 or depths greater than 20 km (cf. Fig.3 left).

Since 2007 the permanent seismic network operating in Portugal has increased in number and quality, currently comprising over 30 stations, the majority being broadband and operated by IPMA-Instituto Português do Mar e da Atmosfera (network code PM), the Portuguese official entity responsible for seismological surveillance, with additional stations belonging to the universities of Lisbon, Évora and Coimbra (network codes LX, IP, SS and WM). Between 2010 and 2012 a temporary network of 20 BB stations operated within project WILAS, an experiment designed to complement the Spanish TOPOIBERIA initiative (cf. Fig3. right; see details in Custodio et al., 2014; Custódio et al., 2015; Diaz et al., 2010).

The data used in this study correspond to the seismic catalogue of IPMA for the period 2000-2014 (cf. Fig.3 left), which was formed using all permanent seismic stations that operated in Portugal in that period coupled with the permanent Spanish stations closer to the border. In the period 2010-2013 the dataset was complemented with readings from the temporary stations of the WILAS project and some of the TOPOIBERIA project (cf. Fig.3 right).

There is some discussion on the usage of off-side network events, i.e., earthquakes with an azimuthal GAP>180º; while a GAP<180º increases the hypocentral solution confidence (e.g. Hunsen, 1999; Kissling et al., 1994), it may exclude valuable information that could be used in the 3D modeling (Koulakov, 2009).

For the data selection criteria we opted for a compromise approach, i.e., increase the GAP limit to 200º but limiting the events to distances of 50 km from the modeled volume (cf. Fig.3 right). The total number of additional events added this way is small, less than 2% of the total, the main advantage being the inclusion of some events at the 180º threshold.

Since the seismicity rate is not uniform, the minimum number of stations/phase readings used in the selection was variable: for events located south of 39ºN that number was set to a minimum of 8 stations and 10 readings of either P- or S-phases, whereas for events located north these numbers were reduced to 6 stations and 8 readings. All events with an RMS>0.7 were checked, eventually with correction or rejection of the phase-picks. This resulted on the selection of 1381 events in the south, and 1282 in the north, reaching a total of 2663 events; since some of these events presented numerical instabilities during the inversion, they were

also rejected, with the final dataset being reduced to 2640 events comprising 28062 P- and 21165 S-phase readings.

The ray-density distribution provided by the combined selected dataset shows a relatively uniform distribution in the south and an irregular distribution in the north, with a hiatus in central Portugal (cf. Figures S1 and S2 in supplementary material). Therefore the 3D grid built for the tomographic inversion has an irregular spacing: south of 39ºN being uniform with an horizontal distance between nodes of 20 km in both directions, whereas to the north it varies between 20 km in the W-E direction and 40-80 km in the N-S direction (cf. Fig.3 right).

The standard tomographic methods assume that picked phases correspond to refracted direct first arrivals which, coupled with the criteria stated above and the expected relation between increasing magnitude and number of events, would imply that all P and S phases of the selected events correspond indeed to first arrivals. However, as the epicentral distance increases, the amplitude of the seismic waves and the signal-to-noise ratio decreases, and the harder it gets to pick the onset of the first arrivals of both the P and S phases. Since the majority of the selected events correspond to microseismicity, rarely exceeding the magnitude of 3.5, the amplitude of the first arrivals is often of the same amplitude of the seismic noise, in particular for distances greater than 150 km where the first arrivals correspond to Pn or Sn phases (cf. Fig.4). Also, the number of stations recording an event depend not only on the magnitude of the event but also on the operational status of the network, which strongly varied along the evaluated period. As a result, some of the available picks do not correspond to first arrivals (Pg, Pn) but actually to secondary arrivals, either refracted or reflected (like the PmP); since the LET method assumes that the P and S picks correspond to first arrivals, the usage of a secondary arrivals will result on unrealistic slower velocity areas in order to accommodate the longer time traveling periods (cf. Fig. 4).

Using the arrivals of the strongest events as guide, all picks corresponding to the more distant events marked as first arrivals but consistent with secondary arrivals (probably Pg or PmP phases) were removed; since these correspond to the deeper travel-paths, penetrating in the lower crust and upper mantle, the consequence was to severely limit the depth

imaging capability. For this reason in the final model the lower crust and upper mantle are outside of the resolved areas.

4. Methodology

The tomographic method used correspond to the widely used and tested code simulps/simul2000 (Thurber and Eberhart-Phillips, 1999; Thurber, 1983). We followed the standard procedure for this method, and for details the reader is referenced to several works published and references therein (e.g. Braeuer et al., 2012; Chiarabba et al., 2009; Dias et al., 2007; Haslinger et al., 1999; Husen et al., 2002; Kissling et al., 2001; Kohler and Eberhart-Phillips, 2002).

4.1. 1D models

The first step in the inversion was to derive a new 1D model to be used as initial input model for the 3D inversion, using the VELEST code (Kissling et al., 1994). Considering the geological heterogeneity in mainland Portugal and the seismicity distribution, the two north and south selected datasets were used to first derive a specific 1D model for each of the regions, followed by a final inversion using the complete dataset to derive the final "best" or minimum 1D model (cf. Fig.5).

All information regarding 1D or 2D models available for Portugal were used for input, namely those used in routine earthquake location at IPMA's (Custódio et al., 2016) or derived on studies previously conducted in Portugal, either from earthquake based analysis (Carrilho et al., 2004; Díaz et al., 2009; Dündar et al., 2016) or deep-seismic soundings experiments (Díaz et al., 1993b; Díaz and Gallart, 2009; Gonzalez et al., 1996; Matias, 1996).

The initial Vp/Vs ratio value, used both during the 1D inversion and as the initial reference value in the 3D inversion, was 1.74 and was determined by a Wadatti diagram (cf. Fig.S3 in supplementary material).

The main differences during the modeling between the two datasets were due to the shallower portion of the models, the southern requiring a slower upper crust. The lower crust present also some sharp differences but these can partially be attributed to instabilities in the solutions due to the exclusion of the more distant arrivals.

The initial RMS of the whole dataset hypocentral parameters was 0.539 s, and following the picks corrections and with the final 1D model, the RMS dropped to 0.251 s, a reduction of 47%. This final RMS value is dominated by the more numerous southern dataset,, the northern events having generally slightly higher RMS values (cf. Fig.S4 and S5 in supplementary material).

4.2. 3D model parameterization

The crustal volume under study was parameterized with the grid of Fig.3, the position of the nodes conditioned by the distribution of ray-density and other indicators, like the DWS and RDE (Kissling et al., 2001).

In the south and extreme north of Portugal, ray-density is relatively uniform, but between 39.5º and 41.5ºN there is a gap due to low seismicity rate and small number of seismic stations; part of the difficulties faced during the 1D and 3D inversion were due to this hiatus in ray coverage and the connection between the two northern and southern blocks. The final grid-nodes disposition, though far from ideal and inducing a north-south stretching in images in the mid-sectors of the model, was the only parameterization that allowed a continuous model with satisfactory resolution.

Besides the displayed horizontal positions, similar planes of grid-nodes were positioned at depths of -1, 1, 4, 8, 12, 16, 20, 24 and 30 km; the external boundary planes placed 500 km for each side of the center of the grid (not shown it the following figures). The already referred figures S1 and S2 in the supplementary material present the ray-density distribution that controlled the grid-nodes set-up.

The total number of nodes is 2640, corresponding to a total of 5280 Vp and Vp/Vs model parameters which, together with the four hypocenter parameters of the 2640 events, result in a total of 10560 unknowns. For the total of 49227 phase readings this leads to an overall over-determination factor of 4.04.

The damping factors for the Vp and Vp/Vs inversions were determined by trade-off curves (Eberhart-Phillips, 1986). The selected values were 300 for the Vp and 150 for the Vp/Vs ratio inversions (Fig.S6 in supplementary material). Other critical parameters selected on a trial-and-error basis were the overall phase weights, with a linear RMS reduction from 0.2 to 0.7 s and cut-off distances, with a linear reduction between 150 and 300 km (according to Fig.4 and Fig. S4).

The final run simultaneously inverting for Vp , Vp/Vs and earthquake location required 4 iterations. The final model, presented in §5, allowed an overall RMS reduction of 58% relatively to the final 1D for the hypocentral parameters, dropping to 0.146 s (cf. Fig.S5 in supplementary material).

Considering the strict criteria applied in the selection of the events, the epicentral distribution obtained from the 3D modeling does not change significantly the sketch resulting from the 1D modeling. The major observable differences being on the depth distribution. While the 1D model tends to have a more homogeneous depth distribution of hypocenters, with more events located at deeper crustal depths, the 3D model has a tendency to cluster the hypocenters in two main ranges: a shallow upper crustal “layer”, with events having depths smaller than 4 km, and an intermediate crustal “layer” where the majority of the hypocenters tend to occur between 7 and 20 km depths, very few events being located at the lower crustal levels (cf. Fig. S7 in supplementary material).

4.3. Model Resolution assessment

The evaluation of the quality of the final 3D model was made both by the usage of synthetic tests, like checkerboard anomalies, and by the analysis of several numerical variables. As

several authors pointed out (Husen et al., 2003; Kissling et al., 2001; Rawlinson and Spakman, 2016), the resolution assessment should not be based on a single test or indicator.

Figure 6 shows the result of the checkerboard sensitivity test output for both the Vp and Vp/Vs models. A synthetic spike-sensitivity test was also performed, not shown since it gave roughly the same indications but with lesser quality. Figures S8 and S9 in supplementary material show the output of the numerical resolution variables calculated from the inversion (Foulger et al., 1995; Toomey and Foulger, 1989), the diagonal of the resolution matrix (RDE) and the Spread Function (SF) distribution. These should be analyzed together with the KHIT and DWS distribution of figures S1 and S2.

Both Fig. 6 and figures S1-S2 and S8-S9 show that the resolution in the upper crustal layers is good, with a few unresolved nodes at the borders of the models, particularly those located at the western edges. Excluding the stretching of the features between latitudes 39º to 41ºN, no significant smearing is observed for layers Z = 1 to 12 km; between 12 and 16 km the resolution starts to decrease with sectors presenting significant smearing or failure to retrieve the initial anomalies.

To prevent ill-resolved areas to affect the geological interpretation, it is prudent to find a way of removing unresolved nodes from the graphical representation of the model. The several figures previously presented, with the numerical resolution parameters and the synthetic tests, do not allow to clearly define the limit between well and poorly-resolved areas.

In order to find a cut-off value for the representation of the resolved nodes of the final 3D model, we followed the approach of Dias et al. (2007): plots of the DWS and RDE values versus the SF value of all nodes and for both the Vp and Vp/Vs models, to define a threshold SF value for resolved nodes (cf. Fig. 7). The higher the SF for a given node, the greater the contribution from nearby nodes and the smaller the reliability of the solution obtained for that node. The graphics in Fig.7 show that the resolution for both models can be considered satisfactory for SF<1.5, and for SF>2.5-3.0 the resolution is null, the SF cut-off value being located in between. The comparison between the output of the several synthetic tests

performed and the distribution of the DWS, RDE, and SF planes, points to a cut-off value of 2.8 for the Vp and 3.0 for the Vp/Vs models.

5. Results

The final Vp and Vp/Vs models are presented in figures 8 and 9. In both cases all node volumes for which their SF is above the respective selected threshold are masked. Each represented horizontal or vertical plane include all relocated earthquakes localized in a slice volume centered in the plane, the thickness of the slice determined by the closest nodes interspacing, usually 20 km for vertical planes (10 km for each side) and 4 km for horizontal planes (2 km for each up-down side). Figure 8 presents both models plotted on horizontal planes, coincident with the horizontal grid XY planes, whereas Figure 9 represents them along selected vertical profiles, either coincident with the XZ or YZ planes (Fig.9a) or along oblique SW-NE or NW-SE profiles (Fig.9b). The horizontal planes are useful mainly to evaluate the lateral horizontal extension of the features, and in particular their correlation with surface geology, whereas the vertical planes are more important to define the vertical extension of the main features and their contrasts. The resolution of the nodes decrease rapidly for depths greater than 20km, with very few of the nodes of the horizontal plane Z=30 km having good resolution; therefore conditioning the depth representation of the models to the upper-middle crust.

As the 1D models already hinted, the analysis of the horizontal maps of Fig. 8 show that the seismic velocities of the upper crust are on average higher in the north than in the south, the south showing much more heterogeneity. Previous work using ambient-noise tomography (Silveira et al., 2013) already showed a tendency of higher group-velocities associated to the north of Portugal and the strong effect associated with the Iberian margin. The vertical distribution of Vp values of the final 3D model fluctuates between 5.7-6.1 km/s in the upper 5km, between 5.8-6.2 km/s in the range 5-10 km, 6.0-6.3 km/s in the range 10-15 km, 6.2-6.5 km/s in the range 15-20 km and 6.4-6.9 km/s in the range 20-25 km, values which are consistent with previous studies carried in the Iberian Massif in particular DSS campaigns (Afilhado et al., 2008; Díaz et al., 1993b; Díaz and Gallart, 2009; Ehsan et al., 2015; Flecha et

al., 2009; Gonzalez et al., 1996; Matias, 1996; Palomeras et al., 2011; Poyatos et al., 2012; Simancas et al., 2004; Téllez et al., 1993; Victor et al., 1980). For depths greater than 25km the model resolution drops dramatically, with only a couple of isolated nodes having a minimum SF value above the defined threshold; therefore, no unequivocal discussion related with Moho depths is possible.

Considering the grid design, namely the uneven spacing between nodes in N-S/Y-direction, coupled with the surface geology, two distinct areas emerge from the obtained tomograms: a northern sector coincident with center-north Portugal and southern Galicia, and a southern sector stretching from the Lower Tagus-Valley until the Algarve, the limit between the two sectors being located around 39.5ºN.

5.1. Northern Portugal and Southern Galicia

This sector, encompassing the region roughly north of 39.5ºN, Y>60 km in Fig.3b, includes the Galicia-Trás-os-Montes Zones (GTMZ), the largest part of the Centro-Iberia Zone (CIZ) and the northern part of the Lusitanian Basin (LB) (cf. Fig.2).

Both figures 8 and 9 show that the seismic structure beneath the CIZ is relatively smooth and homogeneous, the velocities and Vp/Vs ratio varying smoothly when compared with the structure visible to the south beneath the OMZ and SPZ. Such smoothness maybe partially the result of the wider grid spacing, but is nonetheless consistent with previous studies in particular DSS campaigns carried in the area (Díaz et al., 1993b; Díaz and Gallart, 2009; Matias, 1996; Téllez et al., 1993).

In the northern sector, the greatest model heterogeneities are observed in the area around the Spanish-Portuguese border above 41ºN, corresponding to the regions of Minho and Trás-os-Montes in Portugal and southern Galicia in Spain, roughly coincident with the GTMZ positioning (cf.Fig. 2). The Vp values tend to be relatively low (<6.0 km/s) when compared with those from areas slightly to south, ~0.2 km/s smaller, with exception of two high Vp anomalies (~6.2 km/s) roughly at the same latitude of ~42.2ºN (Y=380). The seismicity

distribution in the area seems to be controlled by the position of these two high Vp spots, and confined by the relatively lower Vp areas. The general lower Vp area seems to be confined to the uppermost levels of the crust, vanishing at depths of ~8 km (cf. Fig.8 and profiles A-A´, G-G' in Fig.9a and H-H' and I-I' in Fig.9b). One of the high Vp anomalies is located near the coast, south of the "Rias Bajas" (~8.8ºW), whereas the other is located to the east roughly coincident with the mountain range of the Ourense Central Massif (~7.6ºW). The western high Vp anomaly seems to be detached in depth, with a reduction in Vp that can be perceived at ~8km depth (cf. profile B-B' in Fig.9) whereas the eastern anomaly seems to extend to the deeper crust (cf. profile A-A' in Fig.9). At the shallow layers, the Vp/Vs ratio across the area show some fluctuations around 1.72, but it is at mid-crustal levels that greater variations can be observed and mainly beneath the areas with more seismicity (cf. levels 12 to 20 km depth in Fig.8, and northern profiles in Fig.9). A localized very low Vp anomaly, ~5.7 km/s, is observable at 41.5ºN and 7.7ºW in the plane Z=1km in Fig.8, and apparently extending up to 8 km depth where its shape seems to slightly increase and assume a SSW-NNE orientation.

The general horizontal outline of the referred anomalies disposition in this area (cf. Fig.8), mainly at the shallow layers Z=1km and 4km, suggest a NE-SW alignment that can be correlated with the orientation of the GTMZ and of the Ibero-Armorican Arc (cf. Fig.2a).

The area between 39.5ºN and 41ºN presents more homogenous Vp values, in particular in the area corresponding to the CIZ, but between depths of 8 to 20 km there is evidence of a central region with high Vp values (~6.4 km/s) that seem to be limited between two major tectonic faults, the PTFA and the MVB (cf. Fig.2b), and which has not been previously reported. The ILIHA DSS profiles (Díaz et al., 1993b; Matias, 1996) reported an homogenous crustal structure with no significant lateral variations on the Vp structure with a basically flat Moho; on the other hand, recent PRF studies (Dündar et al., 2016; Mancilla and Diaz, 2015) point to some variation in the Moho topography in the area of the Spanish-Portuguese border, which may be a consequence of this Vp variations.

The Penacova-Régua-Verin (PRV) and the Manteigas-Vilariça-Bragança (MVB) fault systems are some of the major structures of the northern Portugal, in this case extending also into

406 southern Galicia, their signature being clear in the model, the last in spite being located on
407 its eastern border. Both the horizontal planes of Fig. 8 and profile A-A' and H-H' in Fig.9, show
408 a transition between a high Vp area in the west to a low Vp area, the limit roughly coincident
409 with the position of this fault system; the Vp/Vs also presents a similar pattern, though less
410 marked, with a tendency of higher Vp/Vs values east of the fault.
411
412 Along the western part of the model, the transition between the CIZ and the Lusitanian Basin
413 LB is well marked, both on the horizontal planes of the model (Fig.8) and in particular on the
414 vertical W-E profile B-B' and SW-NE profile I-I' of Fig.9ab. This transition is marked by a sharp
415 lateral transition to the western direction in Vp and Vp/Vs values, with a reduction ~0.2 km/s
416 of Vp and strong alternation of Vp/Vs differences >0.4, the anomalies distribution suggesting
417 a contact boundary roughly with a N-S direction. This boundary is consistent with the
418 position of the Porto-Tomar-Ferreira do Alentejo shear zone, PTFA in Fig.2b, the contact
419 between the Variscan structures of the CIZ and the Cenomesozoic structures of the
420 Lusitanian Basin LB (Chaminé et al., 2003; Pais et al., 2012). The shallow layers of profile B-B'
421 seem to define three distinct low Vp anomalies, whose separation appear to be roughly
422 located at longitudes 8.5ºW and 8.0ºW and coincident with the position of some of the fault
423 systems observed in Fig.2b, the NCA and the crossing of the Arr-PTFA faults. The vertical
424 disposition in depth of the anomalies suggest a fault system extending into the lower crust,
425 dipping ~70º to the W.
426
427 Regarding the Vp/Vs ratio, the map present some heterogeneity especially in the upper crust,
428 with values varying between 1.62 and 1.76; for the deeper layers, the heterogeneity reduces
429 somewhat but with a tendency of increasing the average values for values above 1.72. This is
430 in contrast with the results of the study by Dündar et al. (2016), where the average crustal
431 Vp/Vs ratio is usually below 1.75 with the exception of some small anomalies located near
432 the coast. Unlike the Vp anomalies horizontal pattern on Fig.8, the Vp/Vs tends to present an
433 image of N-S alignment of the anomalies, even on the northernmost area where it should be
434 less conditioned by the grid design; the analysis of the Vp/Vs pattern is less obvious than the
435 corresponding Vp, with exception of the clear definition of the margin transition between
436 the LB and the CIZ well defined in Fig.8. Since the major fault systems in this area have an
437 orientation between N-S and NNE-SSW, and considering that the Vp/Vs ratio is more sensible

to lithological variations and in particular fault creep effects (e.g. Eberhart-Phillips and Michael, 1998), this orientation is probably a result of the fault systems signature.

5.2. Southern Portugal (Lower Tagus Valley, Alentejo and Algarve regions)

The region south of 39.5ºN (Y≤60 km in Fig.3b), includes the southernmost part of the Lusitanian Basin LB, the Cenozoic Lower-Tagus-Sado Basin LTSB which includes the Lower-Tagus Valley LTV, the Ossa-Morena OMZ and South-Portuguese Zones SPZ, the contact region CIZ-OMZ and the Algarve Basin AB (cf. Fig.2b).

Due to higher density of information, this region corresponds to the area better sampled by seismic rays, a consequence of the higher seismicity rate and denser seismic permanent network, the closer node disposition allowing a better definition of the model features in terms of spatial size. It is the most geologically heterogeneous region of the study area, which is well marked on the horizontal planes of Fig.8, in particular the shallower ones. To some extent, such heterogeneity was already expected considering that this region comprises the OMZ, the most heterogeneous unit of the Iberian Massif in Portugal, well-marked on the upper layers of the model on Fig.8.

The contrast with the fairly smooth area of the CIZ is evident, although the transition position suggested by the model is not completely coincident with the defined CIZ-OMZ boundary, the Tomar-Badajoz-Córdoba shear zone whose position lies slightly to the NE (TBC in Fig.2b), its expression in the model much weaker. In both the Vp and Vp/Vs models there is a clear contrast roughly coincident with the direction of the seismic alignment visible at ~38.2ºN, located in the Ciborro-Arraiolos region (Cib in Fig.2b), with the TBC lying ~60km to NE being marked by a smaller contrast. East of the Cib alignment and possessing approximately the same orientation, the main structure visible on the field is the Serra da Ossa OA fault, and the couple Cib-SO orientation apparently correspond to an important Vp contrast in the Vp model. On the vertical profiles of Fig.9, a clear sub-vertical Vp contrast associated with the Cib-SOis observed in the upper 10km at longitude ~7.5ºW in C-C', at latitude ~38.9ºN in G-G' and ~200km in K-K'. The area between the Cib-SO alignment and

469 OMZ-CIZ boundary is marked by a low Vp volume observable roughly at latitude ~39.3ºN in
470 G-G' and ~240km in K-K' marked by a gradually increase in Vp values. The TBC is much
471 clearer in the Vp/Vs signature, with the area confined by the Cib and the TBC being marked
472 by high Vp/Vs>1.7. The absence of the TBC on the upper level of the model (Z=1km) may be
473 due to an effect associated with the decrease in the sampling of the crustal volume, since to
474 the NE of the Cib alignment the seismicity rate drops dramatically and thus the inter-node
475 distance increase (Poyatos et al., 2012).
476
477 To the west, the transition between the LB and the OMZ is clear, the separation being well
478 marked by a very low Vp (<5.8 km/s) area roughly coincident with the LTV (cf. Fig.8). Both
479 Fig.8 and profiles C-C' and J-J' show that this low Vp anomaly is limited to the crust's upper
480 10 km, more probably to the upper 5km an effect of the thick sedimentary coverage of the
481 LTSB basin in this area. For depths greater than 10km, no significant lateral transition is
482 observed either on the Vp or Vp/Vs structure nor any significant seismicity alignment is
483 observed in the area.
484
485 Due to the sediment cover of the LTSB, there is some discussion on whether the OMZ or the
486 SPZ stretches until the margin, a suggestion made by ambient noise studies (Silveira et al.,
487 2013). The area between the coast line and the OMZ, roughly between latitudes 38.º-38.5ºN
488 is characterized by low Vp values on the upper crust, overlying a fast middle-lower crust (cf.
489 profiles D-D' and F-F' in Fig.9a), but it is not clear with which zone are these values akin. In
490 Fig.8 the position, shape and values of the low Vp anomalies seem to suggest an horizontal
491 extension of the low Vp associated with the SPZ-OMZ boundary observed eastward.
492
493 To the south of the Cib-SO alignment, a globular diffuse seismic cluster can be observed with
494 no clear alignments. The Vp and Vp/Vs anomalies in this area seem to elongate on a WNW-
495 ESE direction, probably an effect of the Ibero-Armorican Arc (cf. Fig.2a), with some of the
496 stronger anomalies coincident with the globular cluster of earthquakes (cf. Fig.8). This cluster
497 seems to extend in the SW-NE direction, apparently confined to the SE by the Odemira-Avila
498 OA Fault, which itself doesn't seem to correspond to a specific seismic alignment. Profile J-J'
499 (Fig.9b) shows that the seismicity in this area is coincident with high Vp and high Vp/Vs areas,

confined by areas of both low Vp and Vp/Vs and are probably associated with several granitic intrusions in the area.

The position of the OA fault and corresponding contact between Paleozoic and Ante-Ordovician rocks is well marked on the model: in Fig. 8, and within the OMZ, by a high-low Vp transition with the velocity iso-contours roughly parallel to the fault, whereas in Fig.9 it can be perceived at 37.9ºN in profile G-G' and at ~170km in profile J-J'.

At southern OMZ the Vp values are generally lower than at the northern part, enhancing the transition to the SPZ where the velocity values are higher. The SPZ-OMZ transition is marked in Fig.8 mainly at planes above 12 km, with the Vp anomalies contours roughly aligned on a WNW-SSE direction; in profiles F-F' and G-G' of Fig.9a this contact is clear at latitudes of 38.1ºN and 37.8ºN respectively. On profile K-K' of Fig.9b, roughly perpendicular to the contact, this contact is located at ~100km and show also that the low Vp area associated with southern OMZ "bends" to NE suggesting that the SPZ extends beneath the OMZ, as already pointed by the IBERSEIS results (Simancas, 2003). As for the Vp/Vs anomalies the SPZ-OMZ do not have a clear signature, except for the fact that the general WNW-ESE shape of the anomalies observed in Fig.8 inside the OMZ seems to be replaced by less defined orientation is the SPZ. The overall signature of the SPZ-OMZ in Fig.8 is thus perturbed by the superposition of several features, the contact itself, the OA fault and the southern branch of the Lower-Tagus-Sado basin (LTSB).

The South-Portuguese Zone (ZOM) as long been assumed as relatively homogenous (cf. Fig.2), with the eventual exception of the area close to the SPZ-OMZ contact to the northeast, along the Iberian Pyrite Belt, and the southwestern most tip near the Cape of Saint Vicente. The obtained Vp and Vp/Vs models points to a more complex structure instead.

The most striking signature in the models is the apparent W-E segmentation of the SPZ, with a general increase in Vp values from west to east visible in practically all planes of Fig.8 over the resolved areas, and in profile E-E' of Fig.9a. The Vp/Vs also present the same tendency, albeit less clear. The iso-contours of the model suggest a roughly N-S limit not previously

532 reported, butthe fact that there is a seismicity alignment roughly coincident with the W-E
533 variation position in the model suggest that it reflects the presence of a major rheological
534 contact between two distinct blocks.
535
536 While the “fast bloc” occupies all the SPZ area east of this “contact”, the “slow bloc” seems
537 to be also limited by the OA fault, since the SPZ that outcrops near the coast north of the OA
538 fault presents higherVp values akin with the eastern ones.
539
540 The Monchique Massif (M), corresponding to a Mesozoic essentially syenitic massif intrusion,
541 presents a strong signature in the models and also a high seismicity rate cluster, centered on
542 the Massif. Profiles F-F’ and K-K’ in Fig.9 both have a cross-section of the Massif: in the
543 upper 5km, a high Vp anomaly with scarce seismicity is observed, which corresponds
544 probably to the main sienitic body of the Massif, lying above a low Vp anomaly where the
545 majority of the earthquakes are located. Although both vertical profiles seem to suggest
546 high/low Vp/Vs coincident with the referred Vp anomalies, the Vp/Vs planes of Fig.8 point to
547 a greater variability of the Vp/Vs values.
548
549 To the SW of the Massif, there is evidence of significant anomalies in the Vp and Vp/Vs ratios.
550 Although this sector is located on the border of the model, in an area with poor ray-
551 coverage, the suggestion of great heterogeneity is supported by several studies (Dündar et
552 al., 2016; El Moudnib et al., 2015; Gonzalez-Fernandez et al., 2001; González et al., 1996;
553 Matias, 1996; Rocha et al., 2010; Salah, 2013).
554
555 The Monchique Massif, together with the Sintra (S) and Sines (Si) massifs (cf. Fig.2b),
556 composes an alignment of three similar intrusive granitic/syenitic massifs. Unlike Monchique,
557 the ray-coverage of this study do not allow a good sampling of Sintra and Sines, with Sintra
558 located outside the covered area; as for Sines, it lies in the western limit of the model and
559 the shallow high Vp anomaly located in the westernmost side of profile D-D’ in Fig.9a, at
560 9ºW, is probably the signature of the Si massif.
561
562 Finally, there is the low Vp and high Vp/vs signal at the southernmost part of the model,
563 roughly around 8ºW, that is probably the signal of the Mesocenozoic rocks of the Algarve

564 Basin (AB). On average, the Vp values on the AB tend to be slightly than those of the LB but
565 being located on the limit of the model, with only a few nodes sampling the area, do not
566 allow any further conclusion.
567

568 *5.3. Seismicity distribution and active faults*
569

570 To better access the seismicity distribution and eventual relation between alignments and
571 seismic active faults, we decided to add additional events from the original dataset and
572 relocated them with the new 3D model. To keep some confidence in the hypocentral
573 solution, only events recorded at least by four stations and with good azimuthal coverage
574 (GAP<180º) were selected. As result 3735 additional events were obtained and relocated,
575 their epicenters plotted in Figure 10, together with the 2640 used in the inversion process. To
576 discriminate between the two datasets, the events used in the inversion have a symbol
577 slightly bigger and are superimposed over the additional events. The events are plotted over
578 three different depth ranges, defined according to the logic used in Fig. 8: shallow events
579 located in the top of the crust above 2.5 km (the upper plane Z=1 km), mid-crustal events
580 located 2.5-14 km depths (planes Z = 4, 8, 12 km) and deep crustal events for all deeper than
581 14 km (planes Z = 16, 20, 24 km).
582

583 The analysis of Fig.10 shows that the shallower seismicity (Z≤2.5km, Fig.10a) does not define
584 clear alignments with the exception of the one associated with the Cib fault. The clusters
585 around Lugo, in the north in Galicia (~42.8ºN), in most of the Alentejo area between 38ºN
586 and 38.8ºN and around the Monchique Massif (~37.8ºN), are already defined.
587

588 The intermediate depths (Fig.10b), corresponding to mid-crustal seismicity is the one that
589 defines more clearly the majority of the identified anomalies, namely those associated with
590 the PTFA shear zone, PRF and MVB fault systems and the other several faults/alignments
591 (CBo, Po, NCA, CPM, Arr, Cib, MST).In the northern sector the seismicity is distributed, on a
592 first analysis, along some of the well-defined fault systems of Fig.2b: the Porto-Tomar-
593 Ferreira do Alentejo (PTFA) shear zone, the Penacova-Régua-Verin fault zone (PRV) and the

Manteigas-Vilariça-Bragança Fault Zone (MVB), whereas a diffuse seismicity is disseminated in the Minho, and Galicia mainly included in the Galicia-Trás-os-Montes Zone (GTMZ).

On the deeper crustal level (Fig.10c), there is still some seismicity, with some alignments still clear whereas others fade. Seismicity alignments still apparent are those along the PTFA shear zone, the MVB fault system and the NCA, CPM and MST faults. The seismicity over the Cib no longer defines a clear alignment, with the activity reduced to a cluster on the eastern segment of the alignment. The seismicity cluster around the Monchique Massif is still very active.

The association of all this seismicity with the referred fault systems can be seen in Fig.10d. The maps of Fig.10 show clearly that the majority of the hypocenters is confined to the upper-middle crust, with only a few structures extending into the base of the crust.

A note should be added to a the cluster that now appears in Fig.10 in SE Alentejo, around 37.6ºN and 7.9ºW and previously hardly distinguishable in figures 8 and 9. This cluster position is roughly coincident with the area of the Neves-Corvo mine, a massive sulphide deposit with significant amounts of copper and zinc. The majority of the events located at deeper crustal layers correspond to the additional less-constrained ones, most of the well-constrained events used in the inversion having shallow locations; thus, this cluster may reflect the mining activity with explosion, having low magnitudes (M<2.0) being mistaken by small earthquakes although the deeper ones (>15km) can hardly be attributed to that.

6. Discussion

In the area of the Galicia-Tras-os-Montes GTMZ region, the fact that low Vp values are observed in the shallow layers of the model is consistent with hypothesis of being composed by a pile of allochthonous thrust sheets, overlying the autochthonous Central Iberian Zone CIZ The diffuse seismicity of the GTMZ region is not yet completed clarified(Martín-González, 2009; Martínez-Díaz et al., 2006; Vázquez et al., 2008), with some authors suggesting that it could be trigged by some *magmatic diapirs* (Boillot et al., 1980) in depth associated with an

625 intense hydrothermal and magmatic pneumatolytic activity. The activity could also be
626 intensified by the heritage of some of the active faults that controlled the subsidence of the
627 “Rias Bajas” and endorse the indented shape of the littoral border. The existence of several
628 medium temperature hydrothermal springs, some of them with a low to medium geothermal
629 values and mineralizations (Lourenço and Cruz, 2006; Lourenço, 1998), also corroborate
630 these considerations and can explain the observed low Vp associated with the seismicity and
631 the variations in the Vp/Vs ratio in depth.
632
633 The subvertical PTFA shear zone (Chaminé et al., 2003), with N15E to
634 N30Wstrike,concentrates the large majority of events south of GTMZ. It is a major accident
635 of the Iberian Variscan chain that some authors relate with a Cadomian mega structure – a
636 transform fault, reactivated during Variscan orogeny (Ribeiro et al., 2009) and dated to have
637 acted at ca. 208 Ma ago (Gutiérrez-Alonso et al., 2015; Linnemann et al., 2008). Despite the seismic
638 activity along its trace and associated with its northern termination, it does not present
639 significant signatures in the Vp map, only the Vp/Vs ratio showing a hint of its presence, and
640 will thus be discussed in the following section.
641
642 The PRV fault zone is essentially a strike-slip sinistral fault trending N15 to N30E. Its presence
643 is marked by a low-velocity anomaly at the upper crustal levels, roughly at 41.8ºN and 7.6ºW,
644 clearly visible at the Z<8km surfaces(cf. Fig.8) and in profiles A-A’ and E-E’ (cf. Fig.9), and
645 Vp/Vs values slightly lower than 1.7.Displays left kinematic movement during the Cenozoic
646 (locally with a thrust components to W) of over 250 km length, and is an important Variscan
647 inherited structure affecting more recent Quaternary sediments(Cabral, 1989; De Vicente et
648 al., 2011).It has a strong instrumental seismicity record and is associated with various
649 sources of hydrothermal features of hot water (Lourenço and Cruz, 2006; Lourenço, 1998),
650 locally with mantle signature, i.e., Chaves high enthalpy spring, thus explaining the low Vp
651 and Vp/Vs present in the model.
652
653 As described in §5.1, the Centro-Iberian Zone is marked by relatively uniform high Vp values,
654 with the highest values being observed at mid-crustal layers and roughly limited between the
655 PTFA and MVB faults, whereas the Vp/Vs has smooth variations usually above 1.72 and
656 mainly in the shallower crust. The apparent N-S orientation of this high Vp region do not

appear to be completely coincident with that of the faults, which may be due to an effect induced by the model grid, or with the main orientation of the Variscan structures; nonetheless, this anomaly may be reflecting different rheologic areas within the CIZ crust (e.g. between Granites and Schist-Greywacke complexes) that somehow influenced the tardi-variscan development of these set of faults.

The MVB fault system corresponds to a discrete left lateral shear zone, with an NNE-SSW (N10E to N35E) direction, with an estimated length of 230 km and affecting the Variscan crystalline basement. In the central segment of the Vilariça basin reaches the maximum value of 9 km on left lateral component(Cabral, 1989), with some authors suggesting to be the final result of several handling stages from Variscan orogeny to the present (late Quaternary)(Cabral, 1995; Neves et al., 2015; Ribeiro et al., 1990; Rockwell et al., 2009). From them at least 1 km is ascribed as Quaternary Pliocene tectonic events. The Plio-Quaternary activity of the fault is evident with regional geomorphologic expression and the presence of sediments affected (locally with left lateral and thrust components, Cabral, 1995; Neves et al., 2015). The geomorphological criteria shows several indicators of Quaternary activity in this fault/shear zone that attest the left lateral component: scarps well outlined and rectilinear steps, compressional structures, the significant deflection to the left of Douro river and some small steps of river terraces (Cabral, 1995; Rockwell et al., 2009).

As stated above, the transition defined by the MVB fault zone of two volumes within the crust with different Vp values may explain the thinner crustal thickness values obtained from receiver functions studies for stations located in the area (Dündar et al., 2016; Mancilla and Diaz, 2015).

The central area of Portugal, between latitudes of 39ºN and 41ºN, corresponds to the volume less well sampled, due to the reduced number of events and stations and consequently with the lowest ray-density. The relatively smoothness is hence probably partially due to the grid geometry, resulting in N-S elongated anomalies both in the Vp and Vp/Vs ratio.

As previously referred, the PTFA shear zone is one of the main tectonic features of Portugal. It's a roughly N-S oriented contact marking a subvertical tectonic border with uplift of the eastern bloc in a dextral regime), having a sharp signature on the northern part of the model (cf. Fig.8 and profiles A-A' and J-J' in Fig.9). It is a complex and deep shear zone, in some ranges strongly branched (see position of profile B-B' in Fig.9a) and materialized an ancient suture with a long history but it is recognized that is still very active as shown by the current seismicity.

From the juncture with the Tomar-Badajoz-Córdoba shear zone, this fault system extends south although there is some discussion regarding its extension because it is partially covered by the Cenozoic sediments of the Tagus and Sado Basins, the LTSB in Fig2.b (Pais et al., 2012). Some authors suggest an extension to the SW very close to the coast, roughly defining a thin coastal range (Arenas et al., 2016a; Shelley and Bossière, 2000), a suggestion which does not appear to be supported by our results. The lateral Vp contrasts observed in the area between the OMZ and the coast line seems to suggest that the PTFA is defining the western limit of the OMZ and terminating somewhere in the SPZ-OMZ boundary.

The low Vp area associated with the Mesozoic rocks of the Lusitanian Basin show also important seismicity, diverting this activity from the PTFA shear zone and distributed along a system of concurrent faults (cf. Figs.2b and 8): the Nazaré-Condeixa-Alvaiázere(NCA), the Candeeiros-Porto de Mós fault (CPM)and the Arrife Fault – Aires-Candeeiros-Montejunto fault system (Arr).These three faults seem to border the low Vp anomaly block, although the grid does not allow a clear image. While these faults are connected with the rifting stages associated with the creation of the Mesocenozoic domain of the LB(Miranda et al., 2009; Pereira et al., 2016; Ribeiro et al., 1990), they are also inherited from the previous Variscan orogeny geometry, the opening of the Atlantic occurring along the Thetys-Rheic suture zone (Linnemann et al., 2008; Nance et al., 2010; Wilson, 1966).

Within the NCA fault system we can consider two branches, to the west the Nazaré Fault and to the east the Condeixa-a-Nova – Alvaiázere fault system, the separation being marked by the link to the CPM fault as can be seen by the seismicity distribution (cf. Fig.10d).The Sicó-Alvaiázere structure is strongly conditioned by Tardi-Variscan accidents that affected the

720 crystalline basement and whose reactivation influenced the Mesozoic deposition and
721 sedimentary cover (Ribeiro et al., 1979; Rosset et al., 1971). In the eastern edge, some
722 tectonic accidents correspond to roll-overs produced on normal listric fault systems
723 corresponding to an initial extensional regime – the LB (Crispim, 1986; Crispim and Ribeiro,
724 1986). The main massif consists of a set of blocks bordered by faults which sometimes
725 develop syncline and anticline structures. Among these folded structures, some with N70E
726 axial line, there are strike-slip combined structures N30E to N40W (Crispim, 1986; Crispim
727 and Ribeiro, 1986), these orientations consistent with the seismicity alignments and the focal
728 mechanisms observed in the area (cf. Fig.1 and Custódio et al., 2016).
729
730 The CPM fault system, composed by the W Candeeiros and the Porto de Mós-Rio Maior
731 faults, presents a clear geomorphological expression coincident with the observed seismicity
732 alignment in the LB (cf. Fig.10). With a general orientation N40E to N15E show a variable
733 trend reactivation with horizontal and vertical components according to the stress field
734 direction(Ribeiro et al., 1996). They range from essentially left strike-slip faults to normal
735 and/or reverse faults, as shown by the focal mechanisms in Fig.1, with some of them
736 corresponding to transfer faults between sections with different geometric alignments. The
737 varying rheology contrast in the region, due to the presence of saline diapirs intruded in
738 compact limestones, may help explaining the seismicity in this region (Jeanniot et al., 2016).
739
740 The Arr fault system is the largest and one of the most typical thrust fault scarps of Portugal
741 (cf. Fig.2b and Fig.10). Located at the east to southeast area of the Estremadura Limestone
742 Massif, the Mezo-Cenozoic Occidental Border, corresponds to a 35km fault scarp
743 individualized from an at least 150-180 km fault border Estrela-Seia-Lousã SL (basement
744 Variscan lithologies) and Aires-Candeeiros-Montejunto (Mesozoic cover- essentially
745 limestones and mudstones). The Arrife fault scarp (40-100m high) is a thrust with a variscan
746 heritage that imbricates, generally with a high angle, the Cretaceous and Jurassic limestones
747 on top of Tagus Cenozoic sediments(Pais et al., 2012).
748
749 To the east, some seismicity alignments can be observed (cf. Fig.10) coincident with the
750 termination of the MVB fault zone and extending to the SW, confined between the SL and
751 the the Cebola-Bogas Cbo fault systems (Ribeiro and Gonçalves, 2013). The signature of

752 these fault systems, coupled with superposition with the PTFA fault, clear in profile B-B' of
753 Fig.9b show that this seismicity develops deeply into the Variscan basement. The SL fault is
754 considered an active fault (Custódio et al., 2016, 2015) but our results show that one should
755 consider instead the block confined by the SL and the Cbo fault systems.
756
757 To the SE, the Ponsul (Po) fault does not present any evident signature in the tomograms, in
758 spite of a few events being present, which may be partially due to the grid design.
759
760 Regarding the historic seismicity affecting mainland Portugal, the area of the Lower Tagus
761 Valley (northern part of the LTSB in Fig.2) is one of the more critical due to its high
762 population density. It is associated with several significant historical earthquakes (Cabral et
763 al., 2013, 2004; Carvalho et al., 2008; Custódio et al., 2015), from which a major tectonic
764 fault is deduced, the LTV fault system in Fig.2b. The sediment thickness can reach several
765 km's(Carvalho et al., 2016), making difficult a proper study of the crustal structure. To the
766 NW the LTV is bounded by the uplifted Mesozoic Estremadura region, whereas to NE and SE
767 is bounded by the CIZ and OMZ. In our model, the LTV fault area is coincident with a low-
768 velocity area in the upper crust cf. fig.8 and profiles C-C' and J-J' in fig.9), consistent with a ~4
769 km thick basin.
770
771 The Ciborro fault (Cib)seismicity is aligned along an N70W direction parallel to the Serra de
772 Ossa (SO) fault system (Almeida et al., 2005, 2001). This seismicity presents an unusual
773 diffused seismic activity in the regional context, characterized by not only shallow
774 earthquakes but also deeper events, usually with reduced magnitude (M<4) although some
775 events have been recorded with higher magnitudes (M>4). The seismicity can occur in
776 apparently isolated events, main shock-aftershocks sequences or grouped in temporal
777 and/or spatial swarms (Wachilala, 2015). This kind of seismicity stands out from the typical
778 intraplate standard, like two other regions described in this work, the Galiza-Minho and
779 Monchique regions. The focal mechanisms present some homogeneity of strike-slip dextral
780 type (Wachilala, 2015), with the epicenters bordering to the north the Évora Massif, this
781 accident having a geomorphological expression.
782

Magnetoteluric soundings carried in the area showed that these Vp anomalies are coincident with strong resistivity anomalies, in both cases the transition coincident either with the Cib fault or the major alignment of Serra de Ossa SO (Almeida et al., 2005, 2001). However, unlike the Cib alignment, the SO alignment do not present significant seismic activity: this could be related to very different geotectonic domains, to the south related to a high-pressure crustal signature and to the north a deep sedimentary low-grade Palaeozoic basin.

The core of the OMZ, with the associated geological and structural complexity is well represented in observed heterogeneity on obtained tomograms. Such heterogeneity is also observed in the studies conducted in the Spanish side of the OMZ (Ayarza et al., 2010; Carbonell et al., 2004; Palomeras et al., 2011; Simancas et al., 2001, 2003). A strong tectonic inmbrication related with obduction phenomena and high-pressure tectonic events associated with several granitic intrusions in the area (Fonseca et al., 1999) may explain the observed complexity, whereas the concentration of the seismicity may be related with a complex interaction with the Odemira-Ávila OA fault.

The OA fault is one of the major tectonic faults recognized in Western Iberia (cf. Fig.2). In spite of being considered active by some authors(Villamor et al., 2012), it does not present any significant events in this study nor instrumental well-constrained seismic activity recorded (Custódio et al., 2015). The OA major fault cuts with a sinistral shear the Alvito-Viana do Alentejo high-pressure structures located inside the OMZ, an area which shows also some instrumental seismicity related with different rheological properties between blue schists and eclogites and the “Série Negra” black-shales (Fonseca et al., 1999).

The low-velocity anomaly observed in Fig.8 (Z<16km), around 7.5ºW and 38ºN, is coincident with the area immediately south of the SPZ-OMZ contact, and extends up to the Albernoa-Aljustrel-Messejana aligment (AAM in Fig.2b). It is located beneath the “Pulo do Lobo” exotic terrane (Fonseca and Ribeiro, 1993; Vieira Da Silva et al., 2007), and is probably the signal of the mafic rocks associated with the green schists/amphibolitic fácies and some scattered ultramafic outcrops of the Beja-Acebuches ophiolite and the Phyllites and Quartzites outcropping south of the contact.

The seismicity within the SPZ present a diffuse pattern to the east, whereas to the west is concentrated either along a roughly NNE-SSW alignment or a cluster around the Monchique-Massif. The NNE-SSW alignment may be the expression of a branch of the Monchique-Santa

Clara de Sabóia fault (MST in Fig.2b), in spite not being coincident with the position of this fault, and is clearly defined up to ~37.8ºN where it contacts with OA fault. North of the OA fault there is a suggestion of the continuation of an alignment until Torrão ~38.3ºN, but some caution must be taken to assume to be the same alignment. In any case, this Monchique-Santa Clara de Sabóia-Torrão alignment has no expression in the existing geological maps; with an N5E to N10E trend, it can only be referred in the field near S. Martinho da Amoreiras – Sabóia area, which corresponds to a sinistral strike-slip discrete shear fault. To the north is covered by the Sado Basin, part of the LTSB in Fig.2b, but should correspond to an active fault system with a clear geomorphologic expression, bordering to the west the Iberian Pyrite Belt region.

As always the attempt of schematization and geographic systematization difficult some correlation that could be made. Several authors (Shelley and Bossière, 2000 and references therein) mention a possible link between the OMZ and even the southern part of SPZ and the GTMZ zones through the Porto-Tomar-Ferreira do Alentejo fault (PTFA). The attempt to justify the Monchique-Sta Clara de Sabóia alignment with a southward prolongation of the PTFA shear zone has been also recently suggested by other authors (Arenas et al., 2016a; Fernández et al., 2017, 2016; Fernández and Arenas, 2015); however, neither the proposed location, which diverge to the west, nor its signature is evident in our tomograms. In our view, the possible extension GTMZ-OMZ in the form suggested by these authors is not supported by our model.

The low Vp anomaly in western SPZ is limited N-NW by the OA fault, to the south by the strong signal associated with the Monchique Massif and its eastward limit eventually being marked by the MST lineament. This area corresponds essentially to the Brejeira formation ("Grupo de Flysch do Baixo Alentejo", in Oliveira et al., 1979) which is essentially composed by greywacke lithologies and black mud shales, defining a characteristic basin in the southwest SPZ border.

The Monchique Massif (M) is characterized by a still active pneumatolytical hydrothermal intrusion, with water with anomalous mineralization and some low temperature (bellow 60ºC) geothermal springs (Bastos, 2011; Lourenço and Cruz, 2006; Lourenço, 1998), the

847 mineralization indicating very deep circulation – with deep crustal values (González Clavijo
848 and Valadares, 2003; Miranda et al., 2009; Rock, 1978; Valadares, 2004). At the surface the
849 observed seismic cluster is not evidently associated with any kind of alignments or long fault
850 systems. Geomorphological criteria clearly displays some uplift of 300-350m from the
851 Pliocene to the present day, including 100m uplift in the current Quaternary, paleoseismites
852 justifying intense seismic vibration and sedimentary liquefaction and fluidized material in the
853 Quaternary (Dias and Cabral 2002).
854

855 # 7. Conclusions
856

857 In this work, we present the first Local Earthquake Tomography study covering mainland
858 Portugal and part of southern Galicia in Spain. This is one of the studies contributing to the
859 knowledge of the seismic structure of the lithosphere, following the massive deployments of
860 broadband seismic stations by projects WILAS in Portugal (2010-2012) and TOPOIBERIA in
861 Spain (2007-2013).
862

863 Due to the irregular seismic activity rate in Portugal, especially in the north, the observation
864 period of the WILAS project was expanded to include additional data. Thus, the analyzed
865 period spans a period of 15 years, from 2000 to 2014, allowing a good and dense ray
866 coverage of the study area. The data selection criteria were set to increase the maximum
867 confidence in the results as possible: each selected event had to be registered by a minimum
868 of 6-8 stations, depending if it was located in the north or the south, and a minimum of 8-10
869 P or S readings. Also, since for certain epicentral distances several incongruences were
870 detected in the picking, additional criteria was applied to clean the dataset and reduce has
871 much as possible the uncertainty regarding the seismic phases arrival times. The main price
872 paid for such cautious approach was the lack of very long seismic travel-paths, in effect not
873 allowing the imaging of the lower crust.
874

875 The remaining selected dataset, comprising 2640 events recorded over a variable seismic
876 network of over 100 stations both in Portugal and Spain, allowed the calculation of a 3D
877 model with the distribution of Vp and Vp/Vs on a grid with an irregular design. With

878 exception of the mid-lower crustal levels, the model presents a good resolution although
879 with some N-S stretching of the anomalies in the center part of the country.
880
881 The complex history of the assemblage of the crust beneath Western Iberia is well-marked in
882 the final models. The arcuate shape of the Ibero-Armorican Arc can be perceived over the
883 general pattern of the Vp and Vp/Vs anomalies, albeit local perturbations some of which
884 induced by the inversion grid setup. The Vp values are on average higher in the north,
885 decreasing southward and westward into the Iberian margin.
886
887 As should be expected and according to several previous studies, the heterogeneity observed
888 on the surface geology of the Galicia-Tras-os-Montes Zone is well marked in the tomograms,
889 a relatively thin layer over the smoother structure of the Centro Iberia Zone CIZ. The CIZ
890 block confined between the Porto-Tomar-Ferreira do Alentejo shear zone and the Manteigas-
891 Bragança fault have generally higher Vp values to the rest of the CIZ, enhancing the contrast
892 with the Lusitanian Basin to the west.
893
894 The Ossa Morena Zone is the more complex area of our model, its heterogeneity signature
895 increasing to the SW, with a relatively smooth CIZ-OMZ transition as compared with the
896 highly complex SPZ-OMZ transition. Within the OMZ the increase in complexity is marked by
897 the alignment composed by the Ciborro and Serra de Ossa faults, marked by the observed
898 seismic alignment.
899
900 The South Portuguese Zone presents bigger heterogeneity than the surface geology
901 suggested, in particular, a W-E segmentation of its upper crust with a corresponding increase
902 in the Vp values. The SW tip of the model presents significant heterogeneity, besides high
903 seismicity rate around the Monchique Massif, whereas to the SE a diffuse observed
904 seismicity is hardly correlatable with any known surface structure.
905
906 Other significant features are the low Vp values associated with the Mesocenozoic rocks
907 outcropping in the Lusitanian and Algarve basins, and the low Vp and high Vp/Vs values of
908 the sedimentary cover of the Lower-Tagus and Sado Basin.
909

910 The seismicity distribution also displays a complex pattern, mainly reflecting the interaction
911 between inherited Variscan or tardi-Variscan structures, that were reactivated, with more
912 recent fault systems created during the rifting stages of the Atlantic and diapir magmatic
913 intrusions.
914

915 ## Acknowledgments

916
917 The authors are grateful to the Instituto Português do Mar e da Atmosfera (IPMA) for the
918 providing of the catalogue data used in this study. The seismic stations used in the catalogue
919 are owned and/or operated by IPMA (PM), by the IGN-Instituto Geográfico Nacional, Spain
920 (ES), by the GEOFON program of the German Deutsches GeoForschungsZentrum GFZ (GE), by
921 IST - Instituto Superior Técnico (IP), IDL-Instituto Dom Luiz (LX), CITEUC-Centro de de
922 Investigação da Terra e do Espaço da Universidade de Coimbra (SS) and ICT-Instituto de
923 Ciências da Terra, Universidade de Évora (WM). Theinstruments for the WILAS temporary
924 deployment were providedby the Geophysical Instrument Pool of the GFZ Potsdam (GIPP),
925 Germany.The temporary WILAS and IberArray deployment were registeredunder FDSN
926 network codes 8A and IB. The GMT-Generic MappingTools (Wessel and Smith, 1998)were
927 used for figure plotting.
928 The authors wish to acknowledge projects WILAS—WestIberia Lithosphere and
929 Astenosphere Structure (PTDC/CTEGIX/097946/2008) and QuakeLoc-PT—Precise earthquake
930 locations in mainlandPortugal and adjacent offshore (PTDC/GEO-FIQ/3522/2012), both
931 funded by Fundação para a Ciência e Tecnologia, for theirmajor contributions to this work.
932 This is a contribution for project SPIDER—Seismogenic Processes In slowly DEforming
933 Regions (PTDC/GEO-FIQ/2590/2014). This publication was supported by project FCT
934 UID/GEO/50019/2013 - Instituto Dom Luiz.
935

936 ## References

937
938 Afilhado, A., Matias, L., Shiobara, H., Hirn, A., Mendesvictor, L., Shimamura, H., 2008. From
939 unthinned continent to ocean: the deep structure of the west iberia passive continental
940 margin at 38°n. Tectonophysics 458, 9–50.
941 Almeida, E., Monteiro Santos, F., Mateus, A., Heise, W., Pous, J., 2005. Magnetotelluric
942 measurements in SW Iberia: New data for the Variscan crustal structures. Geophys. Res.
943 Lett. 32, 1–4. doi:10.1029/2005GL022596
944 Almeida, E., Pous, J., Santos, F.M., Fonseca, P., Marcuello, A., Queralt, P., Nolasco, R.,
945 Mendes-Victor, L.L., 2001. Electromagnetic imaging of a transpressional tectonics in SW
946 Iberia. Geophys. Res. Lett. 28, 439–442. doi:10.1029/2000GL012037
947 Arenas, R., Díez Fernández, R., Rubio Pascual, F.J., Sánchez Martínez, S., Martín Parra, L.M.,
948 Matas, J., González del Tánago, J., Jiménez-Díaz, A., Fuenlabrada, J.M., Andonaegui, P.,
949 Garcia-Casco, A., 2016a. The Galicia-Ossa-Morena Zone: Proposal for a new zone of the
950 Iberian Massif. Variscan implications. Tectonophysics 681, 135–143.
951 doi:10.1016/j.tecto.2016.02.030

952 Arenas, R., Sánchez Martínez, S., Díez Fernández, R., Gerdes, A., Abati, J., Fernández-Suárez,
953 J., Andonaegui, P., González Cuadra, P., López Carmona, A., Albert, R., Fuenlabrada, J.M.,
954 Rubio Pascual, F.J., 2016b. Allochthonous terranes involved in the Variscan suture of NW
955 Iberia: A review of their origin and tectonothermal evolution. Earth-Science Rev. 161,
956 140–178. doi:10.1016/j.earscirev.2016.08.010
957 Ayarza, P., Palomeras, I., Carbonell, R., Afonso, J.C., Simancas, F., 2010. A wide-angle upper
958 mantle reflector in SW Iberia: Some constraints on its nature. Phys. Earth Planet. Inter.
959 181, 88–102. doi:10.1016/j.pepi.2010.05.004
960 Banda, E., 1988. Crustal parameters in the Iberian Peninsula. Phys. Earth Planet. Inter. 51,
961 222–225. doi:10.1016/0031-9201(88)90048-9
962 Bastos, C., 2011. From sulphur to perfume: spa and SPA at Monchique, Algarve. Anthropol.
963 Med. 18, 37–53. doi:10.1080/13648470.2010.525872
964 Boillot, G., Grimaud, S., Mauffret, A., Mougenot, D., Kornprobst, J., Mergoil-Daniel, J.,
965 Torrent, G., 1980. Ocean-continent boundary off the Iberian margin: A serpentinite
966 diapir west of the Galicia Bank. Earth Planet. Sci. Lett. 48, 23–34. doi:10.1016/0012-
967 821X(80)90166-1
968 Borges, J.F., Silva, H.G., Torres, R.J.G., Caldeira, B., Bezzeghoud, M., Furtado, J.A., Carvalho, J.,
969 2016. Inversion of ambient seismic noise HVSR to evaluate velocity and structural
970 models of the Lower Tagus Basin, Portugal. J. Seismol. doi:10.1007/s10950-016-9564-x
971 Braeuer, B., Asch, G., Hofstetter, R., Haberland, C., Jaser, D., El-Kelani, R., Weber, M., 2012.
972 High-resolution local earthquake tomography of the southern Dead Sea area. Geophys.
973 J. Int. 191, 881–897. doi:10.1111/j.1365-246X.2012.05668.x
974 Cabral, J., 1995. Neotectónica em Portugal Continental, Mem. Inst. Geol. E Min. Lisbon.
975 Cabral, J., 1989. An example of intraplate neotectonic activity, Vilariça Basin, northeast
976 Portugal. Tectonics 8, 285–303. doi:10.1029/TC008i002p00285
977 Cabral, J., Moniz, C., Batlló, J., Figueiredo, P., Carvalho, J., Matias, L., Teves-Costa, P., Dias, R.,
978 Simão, N., 2013. The 1909 Benavente (Portugal) earthquake: Search for the source. Nat.
979 Hazards 69, 1211–1227. doi:10.1007/s11069-011-0062-8
980 Cabral, J., Ribeiro, P., Figueiredo, P., Pimentel, N., Martins, a., 2004. The Azambuja fault: An
981 active structure located in an intraplate basin with significant seismicity (Lower Tagus
982 Valley, Portugal). J. Seismol. 8, 347–362. doi:10.1023/B:JOSE.0000038450.23032.68
983 Carbonell, R., Simancas, F., Juhlin, C., Pous, J., Pérez-Estaún, A., Gonzalez-Lodeiro, F., Muñoz,
984 G., Heise, W., Ayarza, P., 2004. Geophysical evidence of a mantle derived intrusion in SW
985 Iberia. Geophys. Res. Lett. 31, L11601. doi:10.1029/2004GL019684
986 Carrilho, F., Teves-Costa, P., Morais, I., Pagarete, J., Dias, R., 2004. GEOALGAR Project: First
987 Results on Seismicity and Fault-plane Solutions. Pure Appl. Geophys. 161, 589–606.
988 doi:10.1007/s00024-003-02464-3
989 Carvalho, J., Pinto, C., Dias, R., Rabeh, T., Torres, L., Borges, J., Torres, R., Duarte, H., 2016.
990 Tectonic evolution of an intraplate basin: The Lower Tagus Cenozoic Basin, Portugal.
991 Basin Res. 1–22. doi:10.1111/bre.12193
992 Carvalho, J., Rabeh, T., Cabral, J., Carrilho, F., Miranda, J.M., 2008. Geophysical
993 characterization of the Ota-Vila Franca de Xira-Lisbon-Sesimbra fault zone, Portugal.
994 Geophys. J. Int. 174, 567–584. doi:10.1111/j.1365-246X.2008.03791.x
995 Carvalho, J., Rabeh, T., Dias, R., Dias, R., Pinto, C., Oliveira, T., Cunha, T., Borges, J., 2014.
996 Tectonic and neotectonic implications of a new basement map of the Lower Tagus
997 Valley, Portugal. Tectonophysics 617, 88–100. doi:10.1016/j.tecto.2014.01.017
998 Chaminé, H.I., Gama Pereira, L.C., Fonseca, P.E., Moço, L.P., Fernandes, J.P., Rocha, F.T., Flores,

D., Pinto de Jesus, A., Gomes, C., Soares de Andrade, A.A., Araújo, A., 2003. Tectonostratigraphy of Middle and Upper Palaeozoic black shales from the Porto-Tomar-Ferreira do Alentejo shear zone (W Portugal): New perspectives on the Iberian Massif. Geobios 36, 649–663. doi:10.1016/j.geobios.2003.03.002

Chiarabba, C., Piccinini, D., De Gori, P., 2009. Velocity and attenuation tomography of the Umbria Marche 1997 fault system: Evidence of a fluid-governed seismic sequence. Tectonophysics 476, 73–84. doi:10.1016/j.tecto.2009.04.004

Crispim, J.A., 1986. Dinâmica Cársica da região de Ansião.

Crispim, J.A., Ribeiro, A., 1986. Tectónica extensional no bordo leste do Fosso Lusitaniano (área de Ancião). Maleo 2, 17.

Custodio, S., Dias, N. a., Caldeira, B., Carrilho, F., Carvalho, S., Corela, C., Diaz, J., Narciso, J., Madureira, G., Matias, L., Haberland, C., 2014. Ambient Noise Recorded by a Dense Broadband Seismic Deployment in Western Iberia. Bull. Seismol. Soc. Am. 104, 2985–3007. doi:10.1785/0120140079

Custódio, S., Dias, N. a., Carrilho, F., Góngora, E., Rio, I., Marreiros, C., Morais, I., Alves, P., Matias, L., 2015. Earthquakes in western Iberia: improving the understanding of lithospheric deformation in a slowly deforming region. Geophys. J. Int. 203, 127–145. doi:10.1093/gji/ggv285

Custódio, S., Lima, V., Vales, D., Cesca, S., Carrilho, F., 2016. Imaging active faulting in a region of distributed deformation from the joint clustering of focal mechanisms and hypocentres: Application to the Azores–western Mediterranean region. Tectonophysics 676, 70–89. doi:10.1016/j.tecto.2016.03.013

De Vicente, G., Cloetingh, S., Van Wees, J.D., Cunha, P.P., 2011. Tectonic classification of Cenozoic Iberian foreland basins. Tectonophysics 502, 38–61. doi:10.1016/j.tecto.2011.02.007

Dias, N.A., Matias, L., Lourenco, N., Madeira, J., Carrilho, F., Gaspar, J., 2007. Crustal seismic velocity structure near faial and pico islands (azores), from local earthquake tomography. Tectonophysics 445, 301–317. doi:10.1016/j.tecto.2007.09.001

Dias, R., Ribeiro, A., 1995. The Ibero-Armorican Arc: A collision effect against an irregular continent? Tectonophysics 246, 113–128. doi:10.1016/0040-1951(94)00253-6

Díaz, J., Gallart, J., 2009. Crustal structure beneath the Iberian Peninsula and surrounding waters: A new compilation of deep seismic sounding results. Phys. Earth Planet. Inter. 173, 181–190. doi:10.1016/j.pepi.2008.11.008

Díaz, J., Gallart, J., Córdoba, D., Senos, L., Matias, L., SuriÑach, E., Hirn, A., Maguire, P., 1993a. A deep seismic sounding investigation of lithospheric heterogeneity and anisotropy beneath the Iberian Peninsula. Tectonophysics 221, 35–51. doi:10.1016/0040-1951(93)90026-G

Díaz, J., Gallart, J., Córdoba, D., Senos, L., Matias, L., SuriÑach, E., Hirn, A., Maguire, P., 1993b. A deep seismic sounding investigation of lithospheric heterogeneity and anisotropy beneath the Iberian Peninsula. Tectonophysics 221, 35–51. doi:10.1016/0040-1951(93)90026-G

Díaz, J., Gallart, J., Pulgar, J. a., Ruiz, M., Pedreira, D., 2009. Crustal structure beneath North-West Iberia imaged using receiver functions. Tectonophysics 478, 175–183. doi:10.1016/j.tecto.2009.08.003

Diaz, J., Villasenor, a., Morales, J., Pazos, a., Cordoba, D., Pulgar, J., Garcia-Lobon, J.L., Harnafi, M., Carbonell, R., Gallart, J., 2010. Background Noise Characteristics at the IberArray Broadband Seismic Network. Bull. Seismol. Soc. Am. 100, 618–628.

1046 doi:10.1785/0120090085
1047 Dündar, S., Dias, N.A., Silveira, G., Kind, R., Vinnik, L., Matias, L., Bianchi, M., 2016. Estimation
1048 of the Crustal Bulk Properties Beneath Mainland Portugal from P-Wave Teleseismic
1049 Receiver Functions. Pure Appl. Geophys. 173, 1949–1970. doi:10.1007/s00024-016-
1050 1257-4
1051 Eberhart-Phillips, D., 1986. Three-Dimensional Velocity Structure in Northern California Coast
1052 Ranges From Inversion of Local Earthquake Arrival Times. Bull. Seismol. Soc. Am. 76,
1053 1025–1052.
1054 Eberhart-Phillips, D., Michael, A.J., 1998. Seismotectonics of the Loma Prieta, California,
1055 region determined from three-dimensional V p , V p / V s , and seismicity. J. Geophys.
1056 Res. Solid Earth 103, 21099–21120. doi:10.1029/98JB01984
1057 Ehsan, S.A., Carbonell, R., Ayarza, P., Martí, D., Poyatos, D.M., Pérez-Estaún, A., 2015. The
1058 structure and nature of the Moho beneath Central Iberia. Tectonophysics 663, 275–289.
1059 doi:10.1016/j.tecto.2015.08.011
1060 El Moudnib, L., Villaseñor, A., Harnafi, M., Gallart, J., Pazos, A., Serrano, I., Córdoba, D.,
1061 Pulgar, J. a., Ibarra, P., Himmi, M.M., Chourak, M., 2015. Crustal structure of the Betic–
1062 Rif system, western Mediterranean, from local earthquake tomography. Tectonophysics
1063 643, 94–105. doi:10.1016/j.tecto.2014.12.015
1064 Fernandes, R.M.S., 2003. The relative motion between Africa and Eurasia as derived from
1065 ITRF2000 and GPS data. Geophys. Res. Lett. 30, 1828. doi:10.1029/2003GL017089
1066 Fernández, R.D., Arenas, R., 2015. The Late Devonian Variscan suture of the Iberian Massif: A
1067 correlation of high-pressure belts in NW and SW Iberia. Tectonophysics 654, 96–100.
1068 doi:10.1016/j.tecto.2015.05.001
1069 Fernández, R.D., Arenas, R., Pereira, M.F., Sánchez-Martínez, S., Albert, R., Mart??n Parra,
1070 L.M., Rubio Pascual, F.J., Matas, J., 2016. Tectonic evolution of Variscan Iberia:
1071 Gondwana-Laurussia collision revisited. Earth-Science Rev. 162, 269–292.
1072 doi:10.1016/j.earscirev.2016.08.002
1073 Fernández, R.D., Fuenlabrada, J.M., Chichorro, M., Pereira, M.F., Sánchez-Martínez, S., Silva,
1074 J.B., Arenas, R., 2017. Geochemistry and tectonostratigraphy of the basal allochthonous
1075 units of SW Iberia (Évora Massif, Portugal): Keys to the reconstruction of pre-Pangean
1076 paleogeography in southern Europe. Lithos 268–271, 285–301.
1077 doi:10.1016/j.lithos.2016.10.031
1078 Ferrão, C., Bezzeghoud, M., Caldeira, B., Borges, J.F., 2016. The Seismicity of Portugal and Its
1079 Adjacent Atlantic Region from 1300 to 2014: Maximum Observed Intensity (MOI) Map.
1080 Seismol. Res. Lett. 87, 743–750. doi:10.1785/0220150217
1081 Flecha, I., Palomeras, I., Carbonell, R., Simancas, F., Ayarza, P., Matas, J., González-Lodeiro, F.,
1082 Pérez-Estaún, a., 2009. Seismic imaging and modelling of the lithosphere of SW-Iberia.
1083 Tectonophysics 472, 148–157. doi:10.1016/j.tecto.2008.05.033
1084 Fonseca, P., Munhá, J., Pedro, J., Rosas, F., Moita, P., Araújo, A., Leal, N., 1999. Variscan
1085 Ophiolites and high-pressure metamorfism in Southern Iberia. Ofioliti 24, 259–268.
1086 doi:10.4454/ofioliti.v24i2.106
1087 Fonseca, P., Ribeiro, A., 1993. Tectonics of the Beja-Acebuches Ophiolite: a major suture in
1088 the Iberian Variscan Foldbelt. Geol. Rundschau 82, 440–447. doi:10.1007/BF00212408
1089 Foulger, G.R., Miller, A.D., Julian, B.R., Evans, J.R., 1995. Three-dimensional vp and vp/vs
1090 structure of the Hengill Triple Junction and geothermal area, Iceland, and the
1091 repeatability of tomographic inversion. Geophys. Res. Lett. 22, 1309–1312.
1092 Ghose, R., Carvalho, J., Loureiro, A., 2013. Signature of fault zone deformation in near-surface

soil visible in shear wave seismic reflections. Geophys. Res. Lett. 40, n/a-n/a. doi:10.1002/grl.50241
Gonzalez-Fernandez, A., Cordoba, D., Matias, L.M., Torne, M., 2001. Seismic crustal structure in the Gulf of Cadiz (SW Iberian Peninsula). Mar. Geophys. Res. 22, 207–223.
Gonzalez, A., Torne, M., Cordoba, D., Vidal, N., Matias, L.M., Diaz, J., 1996. Crustal thinning in the Southwestern Iberia Margin. Geophys. Res. Lett. 23, 2477–2480.
González, A., Torné, M., Córdoba, D., Vidal, N., Matias, L.M., Díaz, J., 1996. Crustal thinning in the Southwestern Iberia Margin. Geophys. Res. Lett. 23, 2477. doi:10.1029/96GL02299
González Clavijo, E.J., Valadares, V., 2003. O maciço alcalino de Monchique, SW português : estrutura e modelo de instalação na crosta superior. Comun. do Inst. Geológico e Min. 90, 43–64.
Gutiérrez-Alonso, G., Collins, A.S., Fernández-Suárez, J., Pastor-Galán, D., González-Clavijo, E., Jourdan, F., Weil, A.B., Johnston, S.T., 2015. Dating of lithospheric buckling: 40Ar/39Ar ages of syn-orocline strike-slip shear zones in northwestern Iberia. Tectonophysics 643, 44–54. doi:10.1016/j.tecto.2014.12.009
Haslinger, F., Kissling, E., Ansorge, J., Hatzfeld, D., Papadimitriou, E., Karakostas, V., Makropoulos, K., Kahle, H.-G., Peter, Y., 1999. 3D crustal structure from local earthquake tomography around the Gulf of Arta (Ionian region, NW Greece). Tectonophysics 304, 201–218. doi:10.1016/S0040-1951(98)00298-4
Hunsen, S., 1999. Local Earthquake Tomography of a Convergent Margin, North Chile: A Combined On- and Offshore Study, PhD Thesis. ed, Rays. Christian-Albrechts-Universität, Kiel.
Husen, S., Kissling, E., Quintero, R., 2002. Tomographic evidence for a subducted seamount beneath the Gulf of Nicoya, Costa Rica: The cause of the 1990 Mw = 7.0 Gulf of Nicoya earthquake. Geophys. Res. Lett. 29, 1238. doi:10.1029/2001GL014045
Husen, S., Quintero, R., Kissling, E., Hacker, B., 2003. Subduction-zone structure and magmatic processes beneath Costa Rica constrained by local earthquake tomography and petrological modelling. Geophys. J. Int. 155, 11–32. doi:10.1046/j.1365-246X.2003.01984.x
Jeanniot, L., Kusznir, N., Mohn, G., Manatschal, G., Cowie, L., 2016. Constraining lithosphere deformation modes during continental breakup for the Iberia-Newfoundland conjugate rifted margins. Tectonophysics 680, 28–49. doi:10.1016/j.tecto.2016.05.006
Julia, J., Mejia, J., 2004. Thickness and vp/vs ratio variation in the iberian crust. Geophys. J. Int. 156, 59–72. doi:10.1111/j.1365-246X.2004.02127.x
Kissling, E., Ellsworth, W.L., Eberhart-Phillips, D., Kradolfer, U., 1994. Initial reference models in local earthquake tomography. J. Geophys. Res. 99, 19635–19646. doi:10.1029/93JB03138
Kissling, E., Husen, S., Haslinger, F., 2001. Model parametrization in seismic tomography: a choice of consequence for the solution quality. Phys. Earth Planet. Inter. 123, 89–101. doi:10.1016/S0031-9201(00)00203-X
Kohler, M.D., Eberhart-Phillips, D., 2002. Three-dimensional lithospheric structure below the New Zealand Southern Alps. J. Geophys. Res. 107, 2225. doi:10.1029/2001JB000182
Koulakov, I., 2009. Out-of-Network Events Can Be of Great Importance for Improving Results of Local Earthquake Tomography. Bull. Seismol. Soc. Am. 99, 2556–2563. doi:10.1785/0120080365
Linnemann, U., Pereira, M.F., Jeffries, T.E., Drost, K., Gerdes, A., 2008. The Cadomian Orogeny and the opening of the Rheic Ocean: The diacrony of geotectonic processes constrained

by LA-ICP-MS U-Pb zircon dating (Ossa-Morena and Saxo-Thuringian Zones, Iberian and Bohemian Massifs). Tectonophysics 461, 21–43. doi:10.1016/j.tecto.2008.05.002
Lourenço, C., Cruz, J., 2006. Aproveitamentos geotérmicos em Portugal Continental, in: XV Encontro Nacional Do Colégio de Engenharia Geológica E de Minas Da Ordem Dos Engenheiros. pp. 1–9.
Lourenço, M.C., 1998. Recursos Geotermicos de Baixa Entalpia em Portugal, in: 4º Congresso Da Água. pp. 1–11.
Mancilla, F., Diaz, J., 2015. High resolution Moho topography map beneath Iberia and Northern Morocco from receiver function analysis. Tectonophysics 663, 203–211. doi:10.1016/j.tecto.2015.06.017
Martín-González, F., 2009. Cenozoic tectonic activity in a Variscan basement: Evidence from geomorphological markers and structural mapping (NW Iberian Massif). Geomorphology 107, 210–225. doi:10.1016/j.geomorph.2008.12.008
Martínez-Díaz, J.J., Capote, R., Tsige, M., Villamor, P., Martín-González, F., Insua-Arévalo, J.M., 2006. Seismic triggering in a stable continental area: The Lugo 1995–1997 seismic sequences (NW Spain). J. Geodyn. 41, 440–449. doi:10.1016/j.jog.2006.01.001
Matias, L., 1996. A sismologia experimental na modelação da crusta em Portugal Continental. Lisbon.
Matte, P., 2001. The Variscan collage and orogeny (480-290 Ma) and the tectonic definition of the Armorica microplate: a review. Terra Nov. 13, 122–128. doi:10.1046/j.1365-3121.2001.00327.x
Matte, P., 1986. Tectonics and plate tectonics model for the Variscan belt of Europe. Tectonophysics 126, 329–374. doi:10.1016/0040-1951(86)90237-4
Miranda, R., Valadares, V., Terrinha, P., Mata, J., Azevedo, M.D.R., Gaspar, M., Kullberg, J.C., Ribeiro, C., 2009. Age constraints on the Late Cretaceous alkaline magmatism on the West Iberian Margin. Cretac. Res. 30, 575–586. doi:10.1016/j.cretres.2008.11.002
Mueller, S., Prodehl, C., Mendes, A.S., Sousa Moreira, V., 1973. Crustal structure in the southwestern part of the Iberian Peninsula. Tectonophysics 20, 307–318. doi:10.1016/0040-1951(73)90120-0
Nance, R.D., Guti??rrez-Alonso, G., Keppie, J.D., Linnemann, U., Murphy, J.B., Quesada, C., Strachan, R.A., Woodcock, N.H., 2010. Evolution of the Rheic Ocean. Gondwana Res. 17, 194–222. doi:10.1016/j.gr.2009.08.001
Neves, M.C., Cabral, J., Luttrell, K., Figueiredo, P., Rockwell, T., Sandwell, D., 2015. The effect of sea level changes on fault reactivation potential in Portugal. Tectonophysics 658, 206–220. doi:10.1016/j.tecto.2015.07.023
Nocquet, J.-M., 2012. Present-day kinematics of the Mediterranean: A comprehensive overview of GPS results. Tectonophysics 579, 220–242. doi:10.1016/j.tecto.2012.03.037
Oliveira, J.T., Horn, M., Paproth, E., 1979. Preliminary note on the stratigraphy of the Baixo Alentejo Flysch Group, Carboniferous of Southern Portugal and on the palaeogeographic development, compared to corresponding units in Northwest Germany. Comun. dos Serviços Geológicos Port. 65, 151–168.
Pais, J., Cunha, P.P., Pereira, D.I., Legoinha, P., Dias, R., Moura, D., Silveira, A., Kullberg, J.C., Delgado, J.A., 2012. The Paleogene and Neogene of Western Iberia (Portugal): A Cenozoic Record in the European Atlantic Domain. Springer-Verlag, Berlin Heidelberg. doi:10.1007/978-3-642-22401-0
Palomeras, I., Carbonell, R., Ayarza, P., Fernàndez, M., Simancas, J.F., Poyatos, D.M., González Lodeiro, F., Pérez-Estaún, A., 2011. Geophysical model of the lithosphere across the

1187 Variscan Belt of SW-Iberia: Multidisciplinary assessment. Tectonophysics 508, 42–51.
1188 doi:10.1016/j.tecto.2010.07.010
1189 Pereira, R., Alves, T.M., 2013. Crustal deformation and submarine canyon incision in a Meso-
1190 Cenozoic first-order transfer zone (SW Iberia, North Atlantic Ocean). Tectonophysics
1191 601, 148–162. doi:10.1016/j.tecto.2013.05.007
1192 Pereira, R., Alves, T.M., Mata, J., 2016. Alternating crustal architecture in West Iberia: a
1193 review of its significance in the context of NE Atlantic rifting. J. Geol. Soc. London.
1194 jgs2016-050. doi:10.1144/jgs2016-050
1195 Poyatos, D.M., Carbonell, R., Palomeras, I., Simancas, J.F., Ayarza, P., Martí, D., Azor, A.,
1196 Jabaloy, A., González Cuadra, P., Tejero, R., Martín Parra, L.M., Matas, J., González
1197 Lodeiro, F., Pérez-Estaún, A., García Lobón, J.L., Mansilla, L., 2012. Imaging the crustal
1198 structure of the Central Iberian Zone (Variscan Belt): The ALCUDIA deep seismic
1199 reflection transect. Tectonics 31, n/a-n/a. doi:10.1029/2011TC002995
1200 Prodehl, C., Moreira, V.S., Mueller, S., Mendes, A.S., 1975. Deep seismic sounding
1201 experiments in central and southern Portugal, in: General Assembly of the European
1202 Seimological Commission 14th-Berlin. DDR National-Komitee für Geodäsie und
1203 Geophysik, Berlin, pp. 261–266.
1204 Rawlinson, N., Spakman, W., 2016. On the use of sensitivity tests in seismic tomography.
1205 Geophys. J. Int. 205, 1221–1243. doi:10.1093/gji/ggw084
1206 Ribeiro, A., Cabral, J., Baptista, R., Matias, L., 1996. Stress pattern in Portugal mainland and
1207 the adjacent Atlantic region, West Iberia. Tectonics 15, 641–659.
1208 doi:10.1029/95TC03683
1209 Ribeiro, A., Kullberg, M.., Kullberg, J.., Manuppella, G., Phipps, S., 1990. A review of Alpine
1210 tectonics in Portugal: Foreland detachment in basement and cover rocks.
1211 Tectonophysics 184, 357–366. doi:10.1016/0040-1951(90)90448-H
1212 Ribeiro, A., Munhá, J., Dias, R., Mateus, A., Pereira, E., Ribeiro, L., Fonseca, P., Araújo, A.,
1213 Oliveira, T., Romão, J., Chaminé, H., Coke, C., Pedro, J., 2007. Geodynamic evolution of
1214 the SW Europe Variscides. Tectonics 26, n/a-n/a. doi:10.1029/2006TC002058
1215 Ribeiro, A., Munhá, J., Mateus, A., Fonseca, P., Pereira, E., Noronha, F., Romão, J., Rodrigues,
1216 J., Castro, P., Meireles, C., Ferreira, N., 2009. Mechanics of thick-skinned Variscan
1217 overprinting of Cadomian basement (Iberian Variscides). Comptes Rendus - Geosci. 341,
1218 127–139. doi:10.1016/j.crte.2008.12.003
1219 Ribeiro, L.M.J., Gonçalves, A.C.R., 2013. Contributo Para o Conhecimento Geomorfológico e
1220 Geológico da Área Envolvente do Couto Mineiro da Panasqueira. GOT - Geogr. Spat.
1221 Plan. J. 3, 93–116. doi:10.17127/got/2013.3.005
1222 Rocha, J.P., Bezzeghoud, M., Caldeira, B., Borges, J.F., Dias, N., Matias, L., Dorbath, C., 2010.
1223 Tomografia sísmica da litosfera continental algarvia. e-Terra 10, 10–12.
1224 Rock, N.M.S., 1978. Petrology and petrogenesis of the monchique alkaline complex, southern
1225 portugal. J. Petrol. 19, 171–214. doi:10.1093/petrology/19.2.171
1226 Rockwell, T., Fonseca, J., Madden, C., Dawson, T., Owen, L.A., Vilanova, S., Figueiredo, P.,
1227 2009. Palaeoseismology of the Vilarica Segment of the Manteigas-Braganca Fault in
1228 northeastern Portugal, in: Reicherter, K., Michetti, A.M., Silva, P.G. (Eds.),
1229 Palaeoseismology: Historical and Prehistorical Records of Earthquake Ground Effects for
1230 Seismic Hazard Assessment. The Geological Society, London, Special Publications,
1231 London, pp. 237–258. doi:10.1144/SP316.15
1232 Salah, M.K., 2013. Upper crustal structure beneath Southwest Iberia north of the convergent
1233 boundary between the Eurasian and African plates. Geosci. Front. 5, 845–854.

1234 doi:10.1016/j.gsf.2013.10.002
1235 Salah, M.K., Chang, S.-J., Fonseca, J.F.B.D., 2011. Crustal structure beneath the Lower Tagus
1236 Valley, southwestern Iberia using joint analysis of teleseismic receiver functions and
1237 surface-wave dispersion. Geophys. J. Int. 184, 919–933. doi:10.1111/j.1365-
1238 246X.2010.04891.x
1239 Serpelloni, E., Vannucci, G., Pondrelli, S., Argnani, A., Casula, G., Anzidei, M., Baldi, P.,
1240 Gasperini, P., 2007. Kinematics of the Western Africa-Eurasia plate boundary from focal
1241 mechanisms and GPS data. Geophys. J. Int. 169, 1180–1200. doi:10.1111/j.1365-
1242 246X.2007.03367.x
1243 Shelley, D., Bossière, G., 2000. A new model for the Hercynian Orogen of Gondwanan France
1244 and Iberia. J. Struct. Geol. 22, 757–776. doi:10.1016/S0191-8141(00)00007-9
1245 Silveira, G., Afonso Dias, N., Villaseñor, A., 2013. Seismic imaging of the western Iberian crust
1246 using ambient noise: Boundaries and internal structure of the Iberian Massif.
1247 Tectonophysics 589, 186–194. doi:10.1016/j.tecto.2012.12.025
1248 Simancas, J.F., 2003. Crustal structure of the transpressional Variscan orogen of SW Iberia:
1249 SW Iberia deep seismic reflection profile (IBERSEIS). Tectonics 22.
1250 doi:10.1029/2002TC001479
1251 Simancas, J.F.., Carbonell, R., González Lodeiro, F., Pérez Estaún, A., Juhlin, C., Ayarza, P.,
1252 Kashubin, A., Azor, A., Martínez Poyatos, D., Almodóvar, G.R., Pascual, E., Sáez, R.,
1253 Expósito, I., 2003. Crustal structure of the transpressional Variscan orogen of SW Iberia:
1254 SW Iberia deep seismic reflection profile (IBERSEIS). Tectonics 22, n/a-n/a.
1255 doi:10.1029/2002TC001479
1256 Simancas, J.F., Ayarza, P., Azor, A., Carbonell, R., Martínez Poyatos, D., Pérez-Estaún, A.,
1257 González Lodeiro, F., 2013. A seismic geotraverse across the Iberian Variscides: Orogenic
1258 shortening, collisional magmatism, and orocline development. Tectonics 32, 1–16.
1259 doi:10.1002/tect.20035
1260 Simancas, J.F., Carbonell, R., González Lodeiro, F., Pérez-Estaún, A., Juhlin, C., Ayarza, P., Azor,
1261 A., Martínez Poyatos, D., Almodóvar, G.R., Pascual, E., Sáez, R., Kashubin, A., Alonso, F.,
1262 Alvares Marrón, J., Bohoyo, F., Castillo, S., Donaire, T., Expósito, I., Flecha, I., Galadi, E.,
1263 Galindo Zaldívar, J., González, F., González Cuadra, P., Macías, I., Martí, D., Martin, A.,
1264 Martín Parra, L.M., Nieto, J.M., Palm, H., Ruano, P., Ruiz, M., Toscano, M., 2004. The
1265 Seismic Crustal Structure of the Ossa-Morena Zone and its geological interpretation. J.
1266 Iber. Geol. 30, 133–142.
1267 Simancas, J.F., Poyatos, D.M., Expósito, I., Azor, a., Lodeiro, F.G., 2001. The structure of a
1268 major suture zone in the SW Iberian Massif: the Ossa-Morena/Central Iberian contact.
1269 Tectonophysics 332, 295–308. doi:10.1016/S0040-1951(00)00262-6
1270 Sousa Moreira, V., Mueller, S., Mendes, A.S., Prodehl, C., 1978. The deep structure of
1271 southern Portugal, in: Geodinámica de La Cordillera Bética Y Mar de Alborán. University
1272 of Granada, pp. 35–41.
1273 Sousa Moreira, V., Prodehl, C., Mueller, S., Mendes, A.S., 1983. Crustal structure of western
1274 Portugal, in: Bisztricsàny, E., Szeidovitz, G.Y. (Eds.), 17th Gen. Assoc. Eur. Seismol. Comm.
1275 Elsevier B.V., Amsterdam, pp. 529–532.
1276 Téllez, J., Córdoba, D., 1998. Crustal shear-wave velocity and Poisson's ratio distribution in
1277 northwest Spain. J. Geodyn. 25, 35–45. doi:10.1016/S0264-3707(97)00002-1
1278 Téllez, J., Matias, L.M., Córdoba, D., Mendes-Victor, L.A., 1993. Structure of the crust in the
1279 schistose domain of Galicia-Tras-os-Montes (NW Iberian Peninsula). Tectonophysics 221,
1280 81–93. doi:10.1016/0040-1951(93)90029-J

Thurber, C., Eberhart-Phillips, D., 1999. Local earthquake tomography with flexible gridding. Comput. Geosci. 25, 809–818. doi:10.1016/S0098-3004(99)00007-2

Thurber, C.H., 1983. Earthquake locations and three-dimensional crustal structure in the Coyote Lake Area, central California. J. Geophys. Res. 88, 8226. doi:10.1029/JB088iB10p08226

Toomey, D.R., Foulger, G.R., 1989. Tomographic inversion of local earthquake data from the Hengill-Grensdalur Central Volcano Complex, Iceland. J. Geophys. Res. 94, 17497. doi:10.1029/JB094iB12p17497

Valadares, V., 2004. O Complexo Alcalino de Monchique: novos dados de cartografia, geoquímica e geocronologia. Fac. Ciências, Univ. Lisboa.

Vázquez, J.T., Medialdea, T., Ercilla, G., Somoza, L., Estrada, F., Fernández Puga, M.C., Gallart, J., Gràcia, E., Maestro, A., Sayago, M., 2008. Cenozoic deformational structures on the Galicia Bank Region (NW Iberian continental margin). Mar. Geol. 249, 128–149. doi:10.1016/j.margeo.2007.09.014

Victor, L.A.M., Hirn, A., VEINANTE, J., 1980. A Seismic Section Across The Tagus Valley, Portugal - Possible Evolution Of The Crust. Ann. Geophys. 36, 469–476.

Vieira Da Silva, N., Mateus, A., Monteiro Santos, F., Almeida, E., Pous, J., 2007. 3-D electromagnetic imaging of a palaeozoic plate-Tectonic boundary segment in SW Iberian variscides (S Alentejo, Portugal). Tectonophysics 445, 98–115. doi:10.1016/j.tecto.2007.06.006

Villamor, P., Capote, R., Stirling, M.W., Tsige, M., Berryman, K.R., Martínez-Díaz, J.J., Martín-González, F., 2012. Contribution of active faults in the intraplate area of Iberia to seismic hazard: The Alentejo-Plasencia Fault. J. Iber. Geol. 38, 85–111. doi:10.5209/rev_JIGE.2012.v38.n1.39207

Wachilala, P.E.M., 2015. Sismotectónica da região de Ciborro-Arraiolos e sua relação com a Geomorfologia local. Universidade de Évora.

Wessel, P., Smith, W.H.F., 1998. New, improved version of generic mapping tools released. Eos, Trans. Am. Geophys. Union 79, 579–579. doi:10.1029/98EO00426

Wilson, J.T., 1966. Did the Atlantic Close and then Re-Open? Nature 211, 676–681. doi:10.1038/211676a0

Zelt, C. a., Smith, R.B., 1992. Seismic traveltime inversion for 2-D crustal velocity structure. Geophys. J. Int. 108, 16–34. doi:10.1111/j.1365-246X.1992.tb00836.x

Zelt, C. a, Ellis, R.M., 1988. Practical and efficient ray tracing in two-dimensional media for rapid traveltime and amplitude forward modeling. Can. J. Explor. Geophys. 24, 16–31.

FIGURES

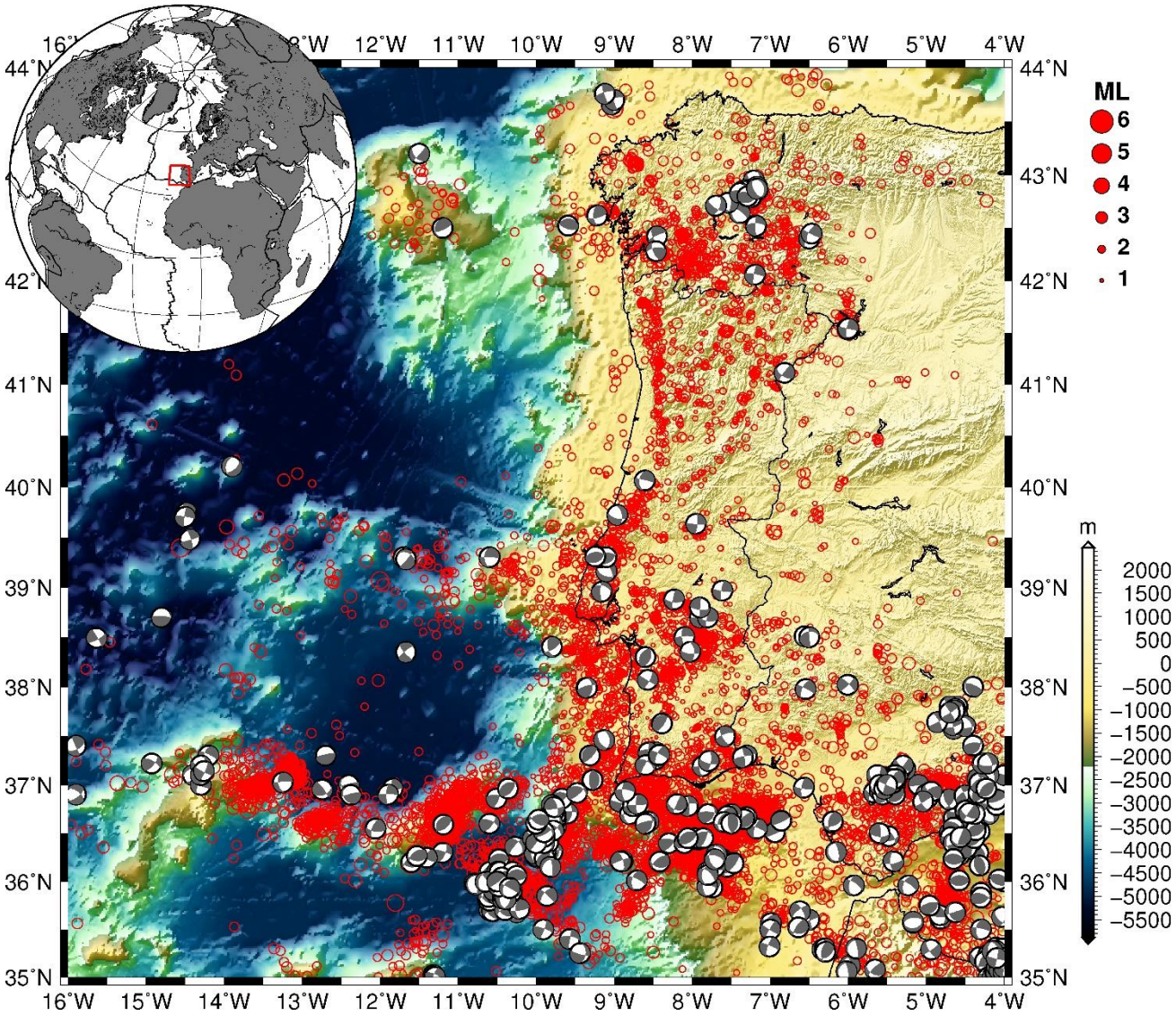

Figure 1 – Recorded seismicity for the period 2000-2014 in the area of Western Iberia, including mainland Portugal, from IPMA's catalogue and focal mechanisms from Custódio et al. (2016). Inset: location of the study area and the relation with the main plate limits.

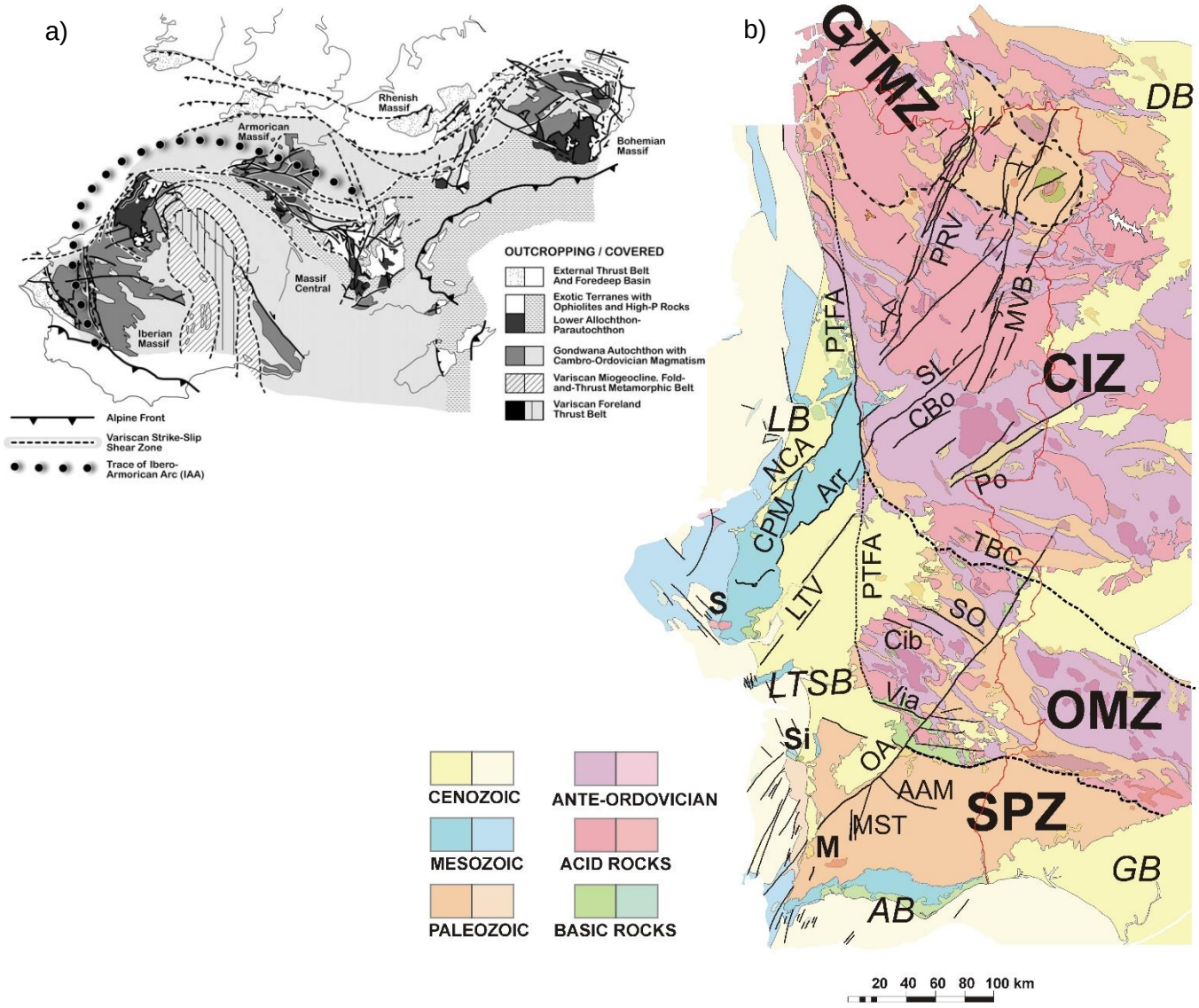

Figure 2 – **a)** Tectonostratigraphic zonation of the Variscan orogen (after Weil et al., 2010) in southwestern Europe including Iberian Peninsula (original modified from Franke, 1989; Martinez-Catalan et al., 2007). Location of Centro Iberian (CIZ), Ossa Morena (OMZ) and South Portuguese Zones (SPZ); **b)** Simplified tectonostratigraphic terrane map of Portugal. It is mainly covered by variscan outcrops, belonging to the Iberian Massif, is tectonically divided into several units: GTMZ Galicia-Tras-os-Montes Zone, CIZ Central Iberian Zone, OMZ Ossa-Morena Zone, SPZ South Portuguese Zone. The western and southern limits of the Massif are defined by Mesocenozoic basins, LB Lusitanian Basin and AB Algarve Basin, with several cenozoic basins partially covering, LTSB Lower Tagus and Sado Rivers Basin, GB Gudalquivir Basin, and DB Douro Basin. The main faults/lineaments/aligments affecting western Iberia are: PTFA Porto-Tomar -Ferreira do Alentejo shear zone; TBC Tomar-Badajoz-Córdoba shear zone; PRV Penacova-Régua-Verin Fault system; MVB Manteigas-Vilariça-Bragança fault system; SL Seia-Lousã fault; CBo Cebola-Bogas fault; Po Ponsul fault; NCA Nazaré-Condeixa-Alvaiázere; CPM Candeeiros-Porto de Mós fault; Arr Arrife fault; LTV Lower Tagus Valley fault system; Cib Ciborro fault; SO Serra de Ossa fault; OA Odemira-Ávila fault; AAM Albornoa-Aljustrel-Messejana Alignment; MST Monchique-Santa Clara fault. The sienitic intrusions of Sintra, Sines and Monchique are marked by S, Si and M (adapted from "Carta Geológica de Portugal", Serviços Geológicos de Portugal, 1992).

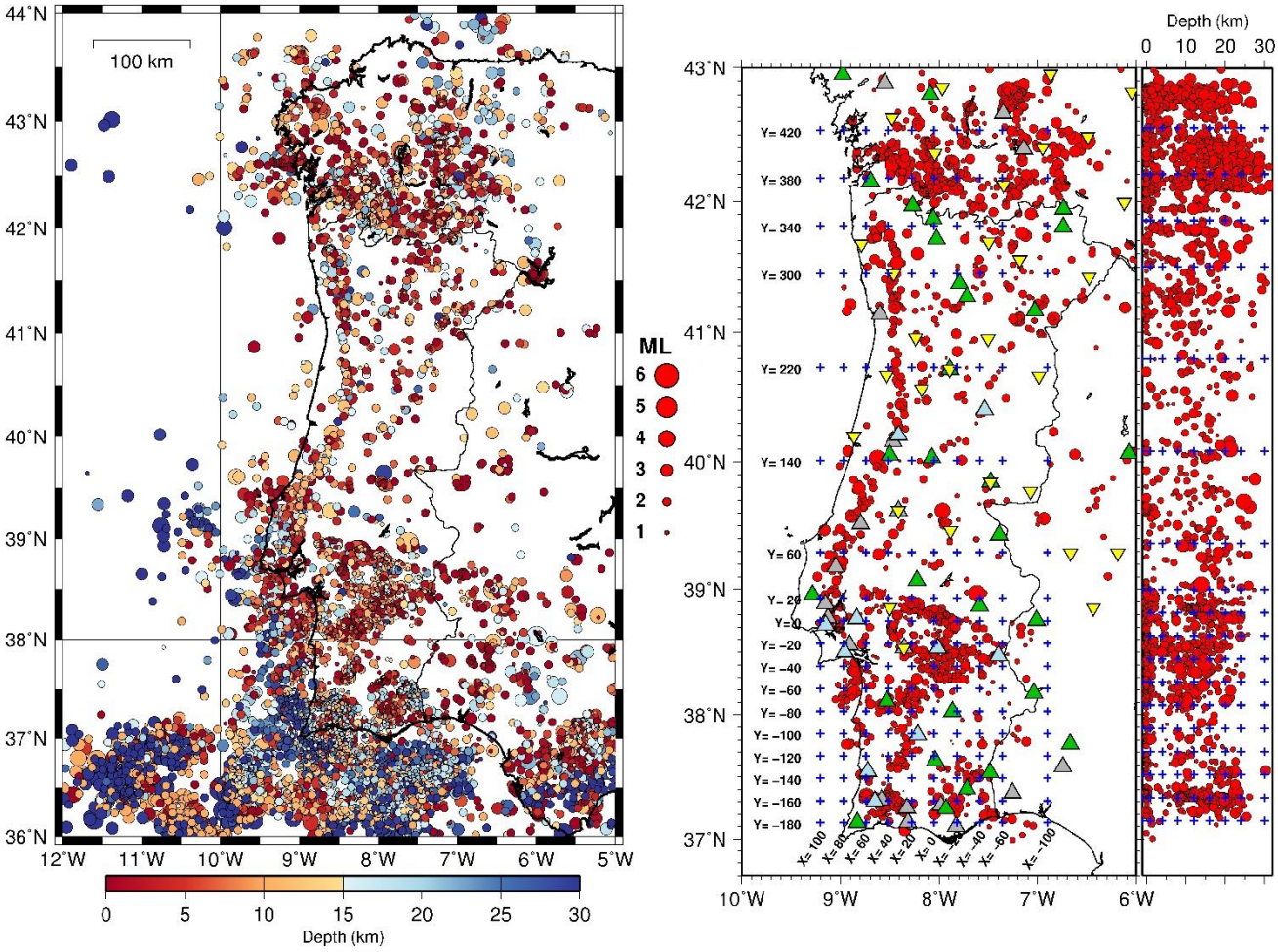

Figure 3 – **Left**: Seismicity epicentral depth distribution in Portugal from IPMA's catalogue 2000-2014; **Right**: seismic networks evolution since 2000 with current permanent active stations (green and light blue triangles) and deactivated stations (grey triangles) in Portugal and Spain; the stations from the WILAS and TOPOIBEIRA temporary deployments 2010-2013 are marked with yellow inverted triangles. Also represented are the 2640 selected events for this study and the position of the grid nodes and corresponding X and Y coordinates.

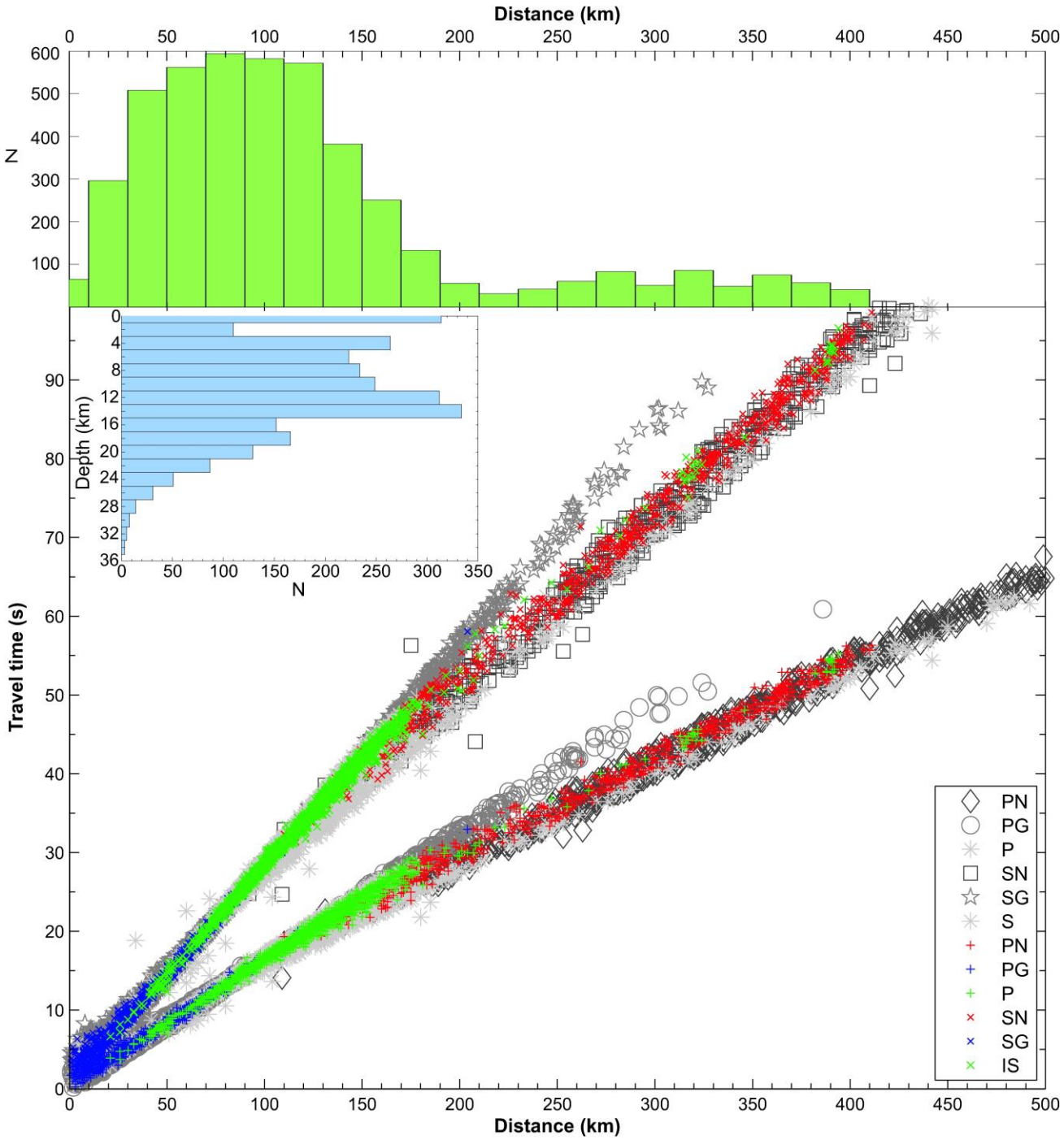

Figure 4 – Histograms of the number of events in terms of distance and depth, bins of 20 and 2 km range respectively, and distance-time graphic of all phases picked as first P and S arrivals in the selected dataset. The labelling corresponds to the existing identification done by the operator in the catalogue (Pg, Pn, P; Sg, Sn, S). In the inversion they are all used as P or S.

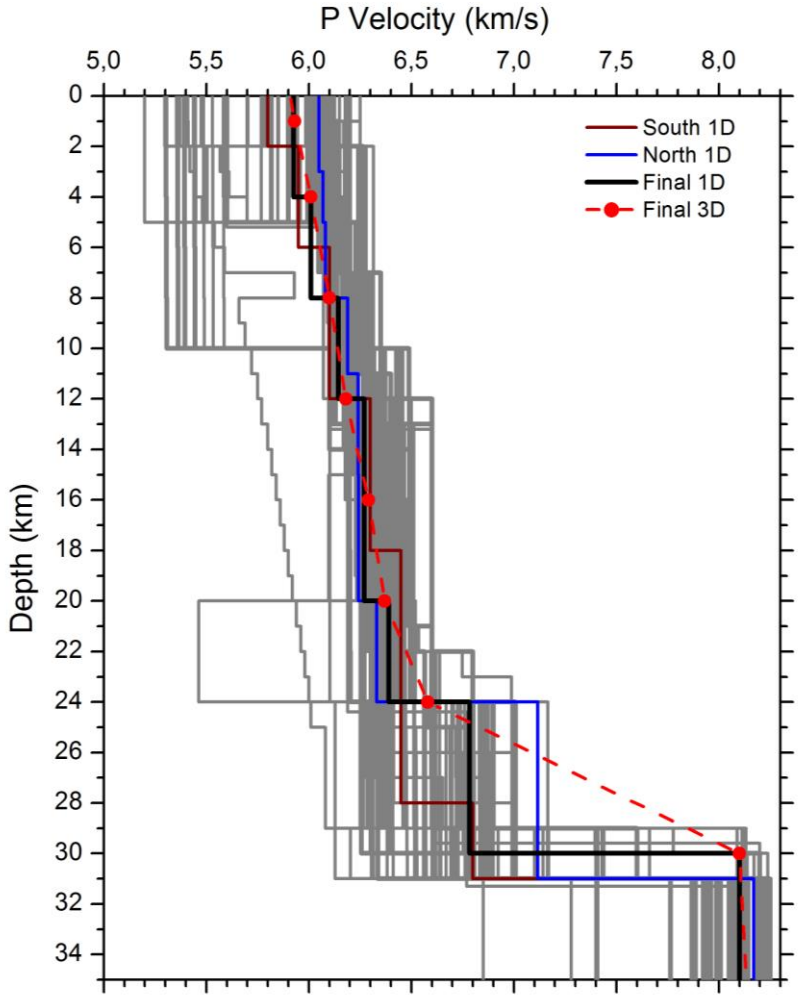

Figure 5 – Graphic Vp-Z with the several tested input models of the 1D inversion with the VELEST code (grey lines). The output models for the two north and south datasets are represented by blue and dark red lines and the final minimum 1D model by a black line, respectively. The adaptation for the input model of the 3D grid is represented by red dots (nodes values) and dashed line (interpolation).

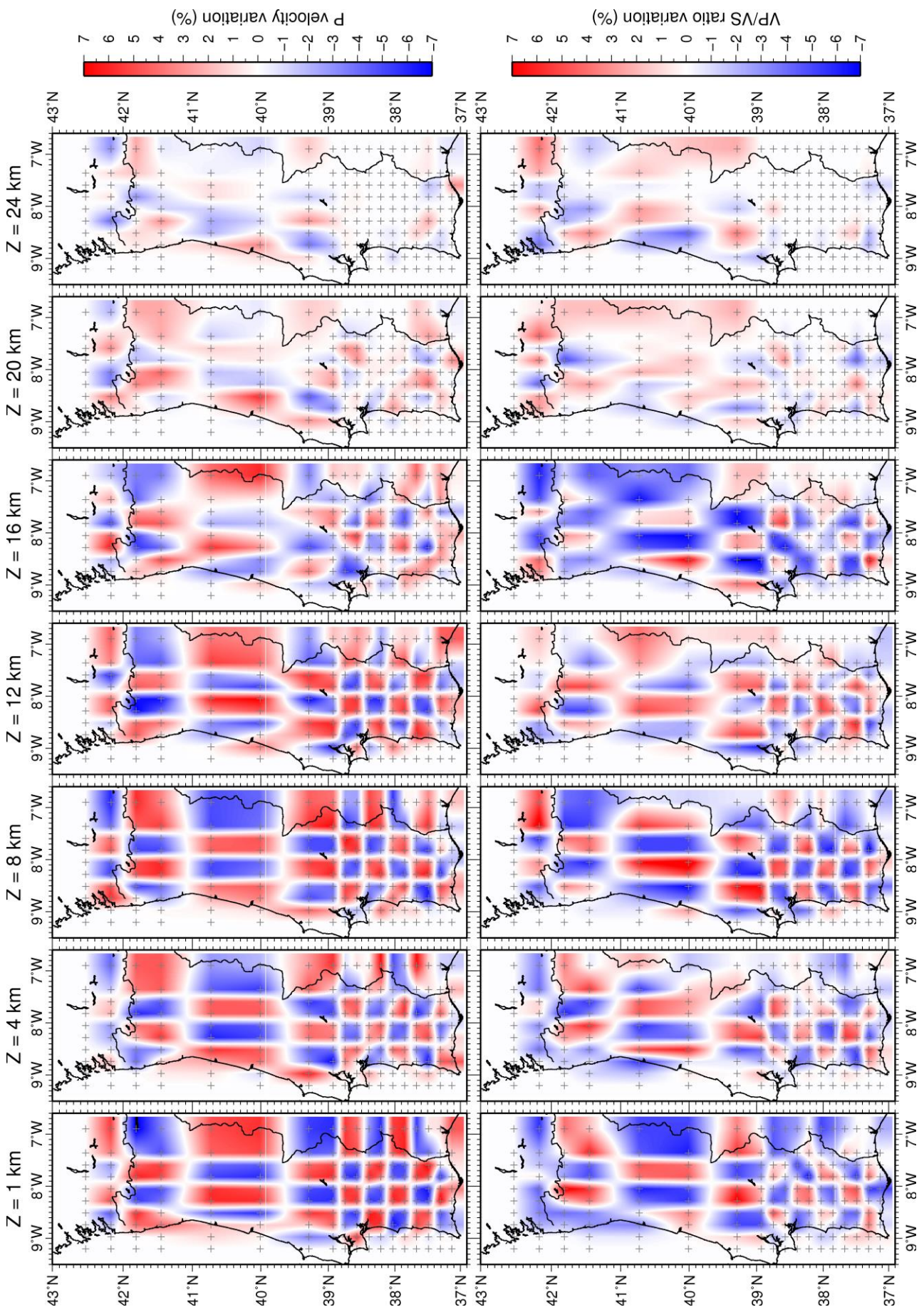

Figure 6 – Checkerboard synthetic tests output for the Vp (top) and Vp/Vs (bottom) models. The represented layers correspond to grid horizontal planes and coincident with the planes of figure 8.

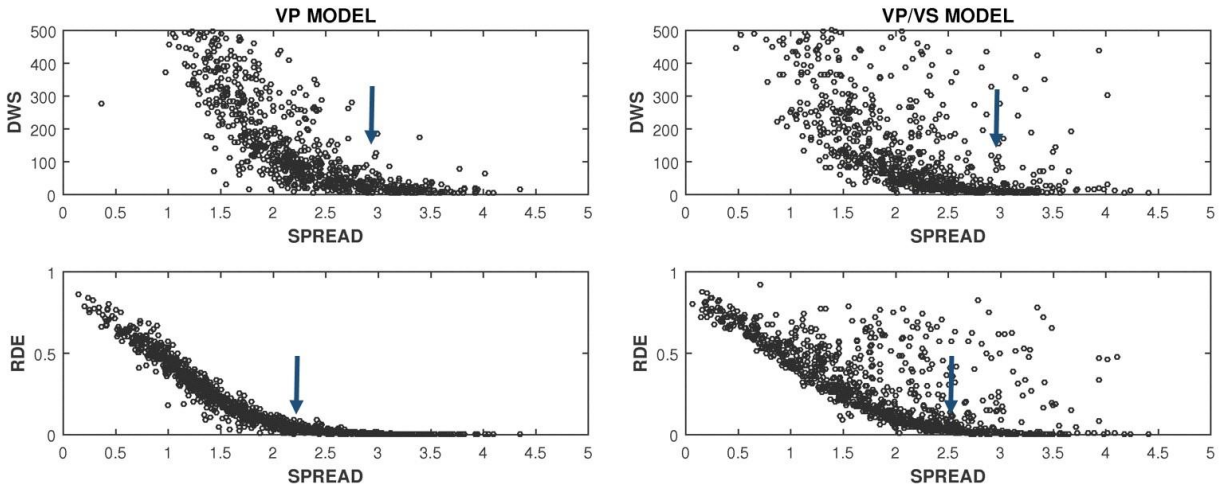

Figure 7 – Plots of the derivative weight sum (DWS) and diagonal element of the resolution matrix (RDE) versus the spread function (SF) values for the Vp (left) and Vp/Vs (rigth) models. The arrows point to the selected threshold values of SF.

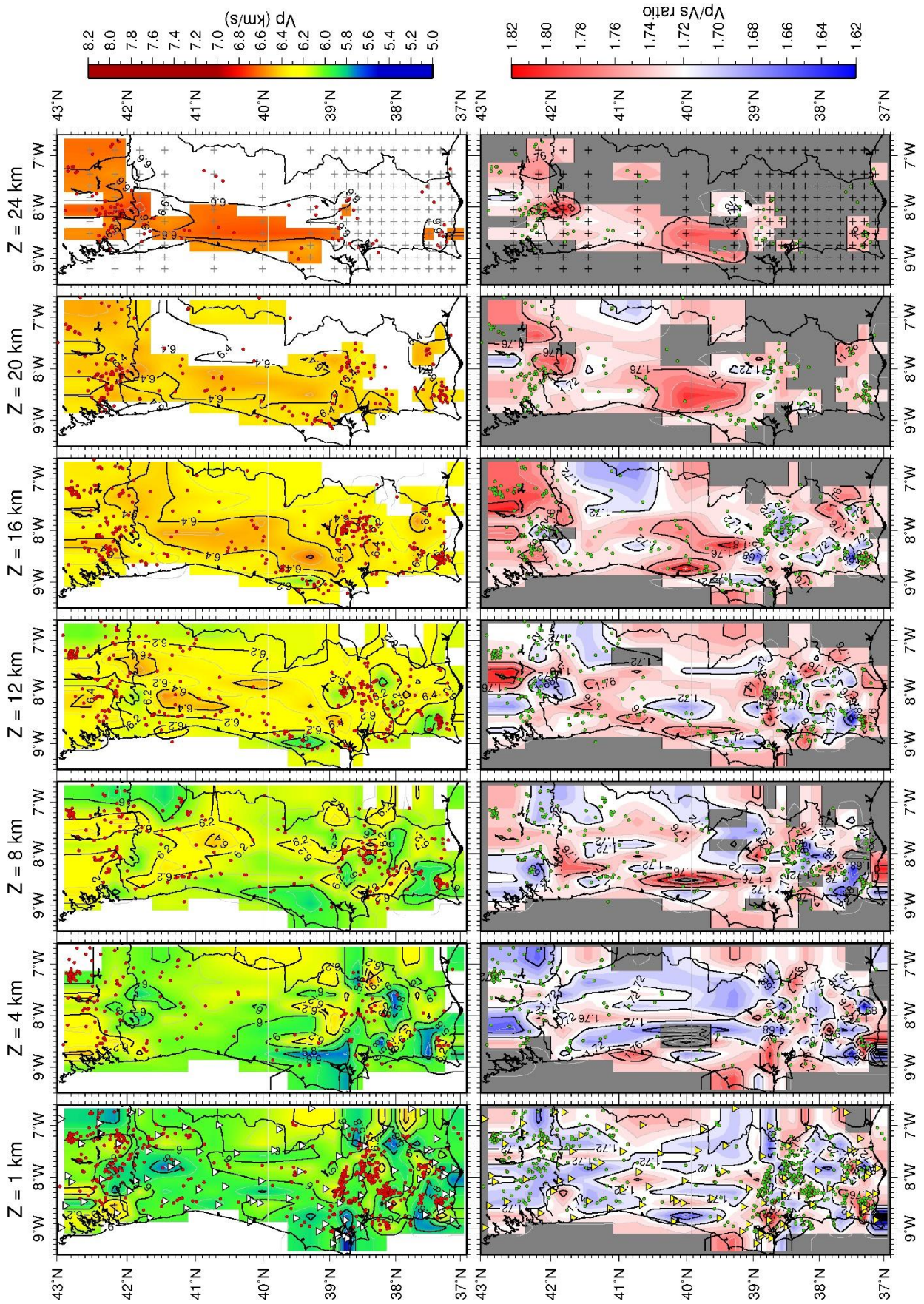

Figure 8 – Final 3D Vp and Vp/Vs models for mainland Portugal and surrounding areas. All nodes with SF higher than the cut-off value (2.8 for Vp, 3.0 for Vp/Vs) are masked. Models represented on seven horizontal XY planes coincident with the grid nodes position, excluding planes Z=-1 and Z=30 km. The relocated earthquakes projected in each layer correspond to events located in a volume +/- 2km around the layer, with exception of the upper 1 and 4 km layers, whose separation is located at 2.5km depth, and the deeper layer which contain all events deeper than 22 km.

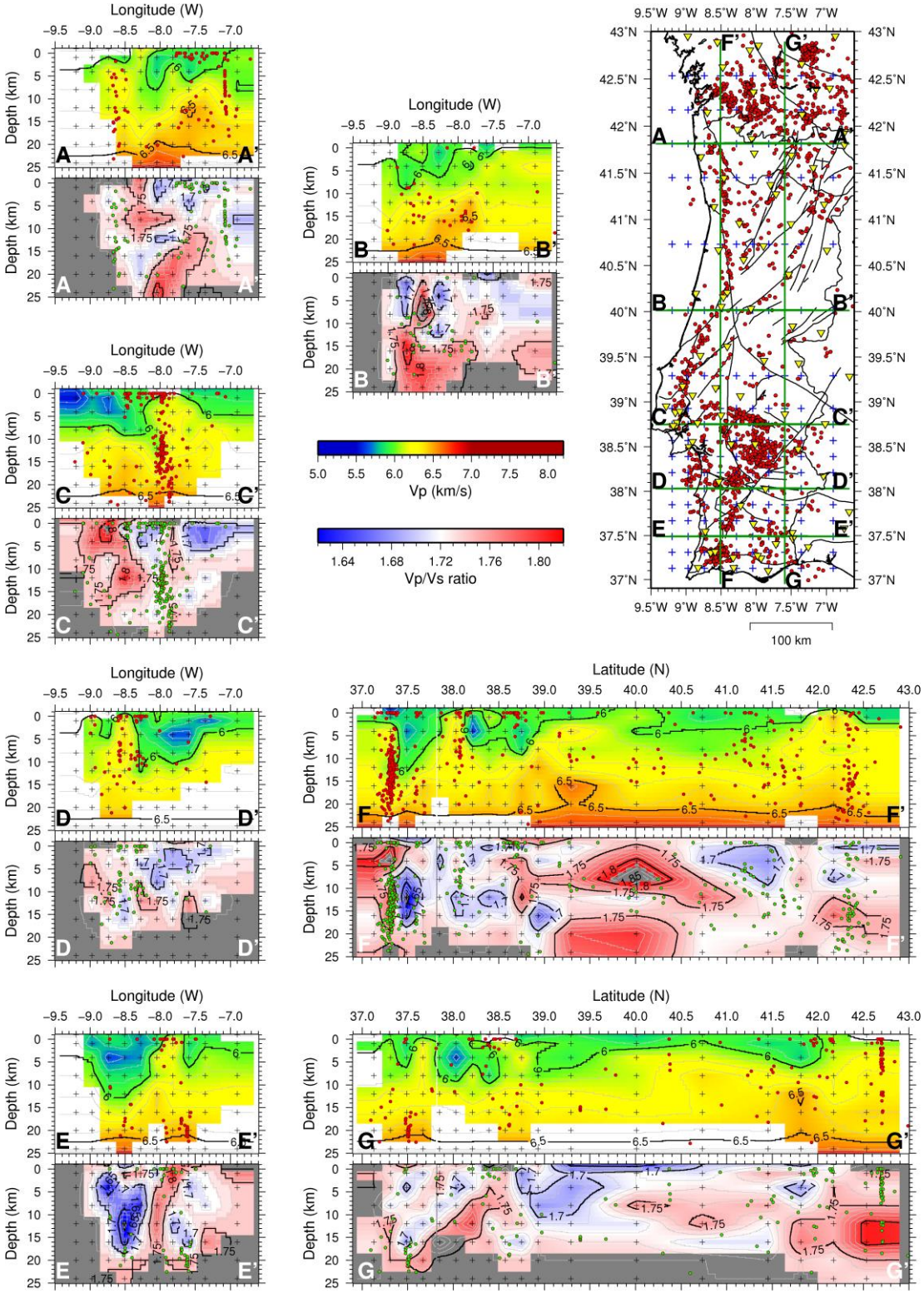

Figure 9a – Vertical profiles of the final 3D Vp and Vp/Vs model. The upper right map presents the relocated epicenters together with the stations and grid, and the position of seven vertical profiles, five W-E along constant latitude (A-A' to E-E') and two N-S along constant longitude (F-F' and G-G'). All profiles are coincident either with XZ or YZ vertical node-planes.. Nodes with SF higher than the cut-off value (2.8 for Vp, 3.0 for Vp/Vs) are masked. The relocated earthquakes projected in each profile correspond to events located in a volume +/- 10km around the slice, with exception of the northern profiles A-A' and B-B' for which the volume is expanded to +/- 20km due to the greater internode distance. Vertical exaggeration of 5:1.

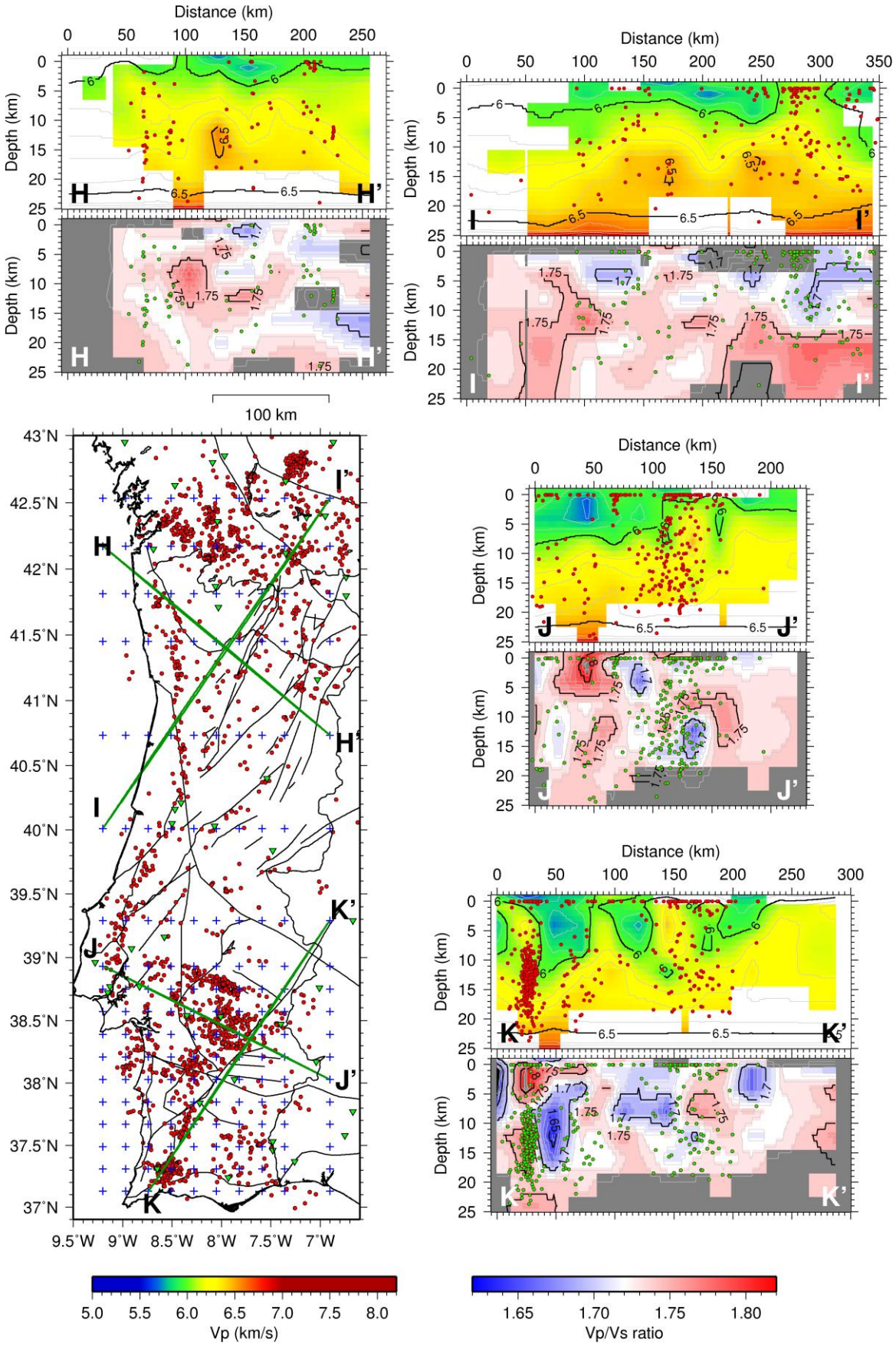

Figure 9b – Vertical profiles of the final 3D Vp and Vp/Vs model. The bottom left right map presents the relocated epicenters together with the stations and grid, and the position of four vertical profiles oblique to the grid, of either SW-NE or NW-SE directions. Nodes with SF higher than the cut-off value (2.8 for Vp, 3.0 for Vp/Vs) are masked. The relocated earthquakes projected in each profile correspond to events located in a volume +/- 10km. Vertical exaggeration of 5:1.

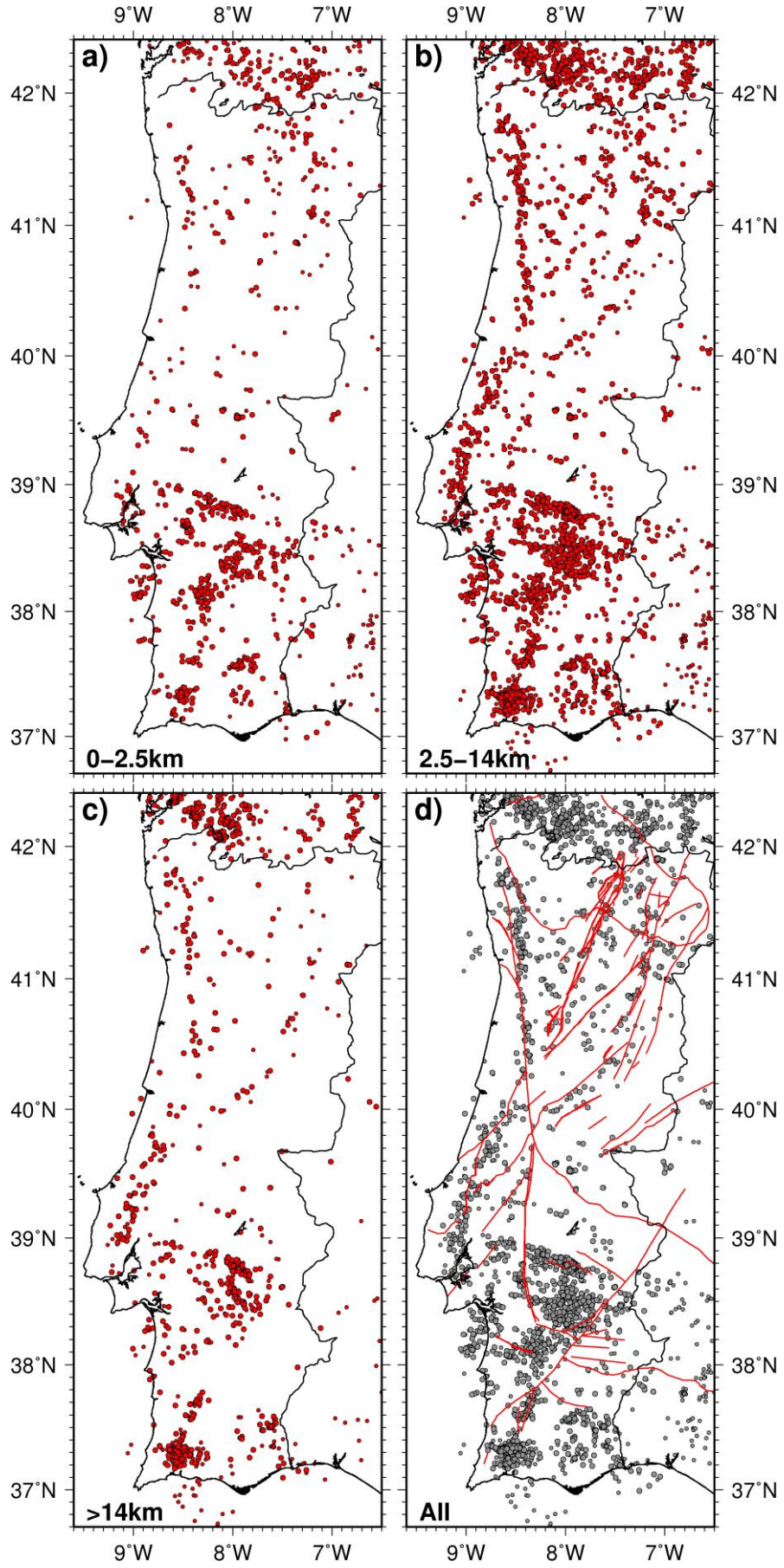

Figure 10 – Map of seismicity distribution of 6375 events, over three depth ranges: a) shallow (≤2.5km); b) upper-mid crust (2.5-14 km); c) lower crust (>14km); d) superposition of the entire dataset with the lineaments and faults of figure 2. The additional events relocated with the 3D model are represented with a smaller circles size (see text for details.